P. A. Kralchevsky, K. D. Danov, Interactions between Particles at a Fluid Interface, In: *Nanoscience: Colloidal and Interfacial Aspects,* V. M. Starov, Ed.; CRC Press, New York, 2010; Chapter 15, pp. 397-435.

15. Interactions between Particles at a Fluid Interface

by Peter A. Kralchevsky and Krassimir D. Danov

Dept. of Chemical Engineering, Faculty of Chemistry, Sofia University, Sofia 1164, Bulgaria

CONTENTS

15.1 INTRODUCTION

The attachment of a particle to the boundary between two fluid phases is usually accompanied by interfacial deformation near the particle (meniscus formation). The overlap of such two deformations gives rise to lateral capillary interaction between the particles.[1–10] As a rule, the lateral capillary force between similar particles is attractive and brings about particle aggregation and ordering, and plays an important role in the production of various two-dimensional structures,[9–12] which is the main reason for the growing interest in this area during the last decade. The obtained structures have found numerous applications for producing photonic crystals;[13,14] photo- and electro-luminescent semiconductor materials;[15,16] nanostructured surfaces for photoelectrochemical and photocatalytic processes;[17,18] optical elements, such as diffraction gratings and interference filters;[19,20] micropatterning by non-densely packed interfacial colloidal crystals;[21,22] paint coatings of new optical properties;[23,24] samples for electron microscopy of viruses and proteins;[25,26] sensors in analytical chemistry;[27,28] miniaturized immunosensors and immunoassays;[29,30] nano-lithography and micro-contact printing;[31–33] production of structured porous (including nanoporous) materials by using colloid crystal templates;[34–36] and so on.

So far, four different physical reasons for the appearance of interfacial deformations (menisci) have been identified. First, for floating "heavy" particles of size greater than ca. 10 μm, the particle weight (together with the Archimedes force) gives rise to an interfacial deformation and lateral capillary attraction (flotation force);[1,3,6,8,9,37] (see Section 15.2.1.)

Second, menisci appear also around colloids that are partially immersed in a liquid film (film on a substrate or a free film) because of the different wettability of the particles by the two neighboring fluid phases.[4,5,7–10,38] The respective capillary attraction (immersion force) was found to produce two-dimensional aggregation and ordering of micrometer- and submicrometer-sized particles,[11,12,39–42] and even of viruses and proteins.[9,25,26] Similar forces are operative between inclusions in phospholipid membranes;[9,43–45] (see Sections 15.2.4–15.2.6).

Third, interfacial deformations can be produced by an undulated contact line on the particle surface due, for example, to surface roughness[9,46] or to non-spherical particle shape (ellipsoids, polyhedrons, etc.). [47–53] Mathematically, the shape of the undulated contact line could be expanded in Fourier series, and depending on the leading terms in this expansion, we

deal with interactions between capillary "dipoles", "quadrupoles", "hexapoles", and other capillary "multipoles";[10,54–56] (see Sections 15.2.2 and 15.4).

Fourth, interfacial deformations can be produced by electric charges at the particle surface. Like-charged particles electrostatically repel each other. They are expected to also experience capillary attraction due to the overlapping of the menisci formed around them. The balance of the latter two forces would lead to the appearance of an energy minimum, corresponding to the equilibrium position of the particle in a two-dimensional colloid lattice.[57] The electrodipping force and the electric-field-induced deformation of the liquid interface around a charged particle of radius about 250 μm have been experimentally observed and theoretically investigated.[58–60] Experiments show that the motion of two such particles toward each other on a liquid interface indicates the presence of an additional attractive force;[61] (see Section 15.2.3, 15.5 and 15.6).

Most of the experimentally observed electric effects with particles at oil/water and air/water interfaces are due to the presence of electric charges at the boundary particle/nonpolar fluid (oil, air).[58–70] Because of the absence (or very low concentration) of ions in the nonpolar fluid, the electric interaction between two particles across the nonpolar phase are not screened. Consequently, the electric repulsion between like-charged particles has a long-range Coulombic character and may lead to the formation of two-dimensional colloid-crystal lattices of relatively large interparticle spacing.[22,62–70] This type of interactions is important also for the properties of particle-stabilized (Pickering) emulsions.[65,68,71]

Theoretical description of the electric force and of the meniscus shape around a *single* charged particle has been published.[58–60] Different results were reported on the *two-particle* problem, which had been a subject of debates in the literature.[72–80] One of the difficulties related to this problem is that the particle electric field affects the meniscus shape not only through the normal force exerted on each particle, but also through the electric pressure (described by the Maxwell stress tensor), which is acting over the liquid interface around the particles. The predictions of the available theoretical models depend on the form of the postulated expression for the free energy of the system and on the type of the used truncated asymptotic expansions or other perturbation procedures. Different approaches have lead to the conclusion that the electric-field-induced capillary force is attractive, but it has been unclear whether it could prevail over the direct electric repulsion between like-charged particles. In

the meantime, the number of experimental indications for the action of attractive forces between particles at liquid interfaces keeps increasing.[61,66,67,81–84]

In the present chapter, we first give a brief review on the different kinds of lateral capillary forces (Section 15.2). Next, we present a general theoretical approach, which can be applied for theoretical description of all kinds of lateral capillary forces (Section 15.3). This approach is further applied to quantify the force and energy of interaction between capillary multipoles of various order; the derived expressions (Section 15.4) are more general than previously published ones.[54–56] Then (Section 15.5), we address the issue about the electric-field-induced capillary force. We consider the case of charges, which are located on the particle/nonpolar-fluid interface and uniformly distributed over it. Asymptotic expression for the interaction force is derived in the form of power expansion, which predicts that in the considered case the total force is repulsive, that is, the electric repulsion between like-charged particles is stronger than the electric-field-induced capillary attraction. Finally (Section 15.6), we consider the case of anisotropic distribution of charges on the particle/nonpolar-fluid interface. The anisotropy of surface charges engenders a deformation in the liquid interface, which is equivalent to a "capillary quadrupole". The interplay of this quadrupolar deformation with the gravity-induced "capillary charge" of the particles, gives a quantitative explanation of the long-range attraction between floating particles, which was experimentally established in Ref. 61. The latter case gives an example for a system, in which the capillary attraction prevails over the electric repulsion.

15.2 Lateral Capillary Forces between Particles Attached to an Interface

As mentioned above, when a colloidal particle is attached to a liquid interface, the latter usually deforms in the vicinity of the particle. The overlap of the interfacial deformations (menisci) engendered by two particles gives rise to lateral capillary force between them (Figure 15.1). The range of these capillary forces is usually much longer than the range of the van der Waals and double-layer surface forces.[1–10] As mentioned above, lateral capillary forces play an important role for the production of two-dimensional (2D) arrays of colloidal particles, protein globules, viruses, and so on.[9–12,25,26] Depending on the physical origin of the

interfacial deformation created by the particles, we can distinguish several kinds of lateral capillary forces, which are illustrated in Figure 15.1 and considered separately below.

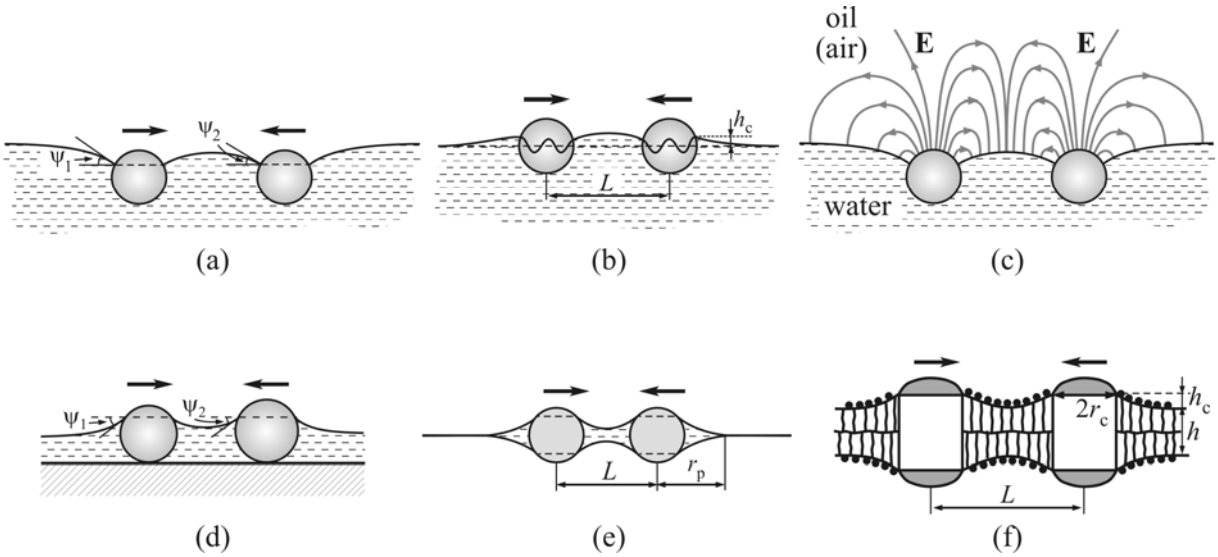

FIGURE 15.1 Kinds of lateral capillary forces between particles attached to liquid interfaces. (a) Flotation capillary force between two floating particles that deform the liquid interface because of their weight. (b) Force between "capillary multipoles" due to the overlap of interfacial deformations engendered by undulated contact line on the particle surface. (c) Electric-field-induced capillary force between two charged particles. (d) Immersion capillary force between particles captive in a liquid film: the interfacial deformation is due to the wettability of particle surface. (e) Capillary force in the case of finite menisci: when the particle diameter is much greater than the film thickness, the meniscus around each particle and the range of action of the capillary force is finite. (f) Inclusions (e.g., integral membrane proteins) in a lipid bilayer (membrane): the thickness of the inclusion can be greater (or smaller) than the thickness, h, of the non-disturbed lipid bilayer; the overlap of the deformations around the inclusions leads to an attraction between them.

15.2.1 Flotation Capillary Forces

First, the interfacial deformation around two floating particles can be due to gravitational effects, that is, the particle weight minus the buoyancy force (Figure 15.1a). In this case, we are dealing with a gravity-induced lateral capillary force,[1,3,6] which was called for the sake of brevity as *flotation force*.[7] To produce a significant interfacial deformation, the particle weight should be large enough. The flotation capillary force is essential for particle diameters greater than 5–10 μm depending on the particle and liquid-phase mass densities.[6] The meniscus shape around an isolated particle of rotational symmetry is described by the expressions:[85,86]

$$\zeta(r) = QK_0(qr), \qquad q \equiv (\Delta\rho g/\gamma)^{1/2}. \tag{15.1}$$

Here, the function $z = \zeta(r)$ describes the meniscus profile; r and z are cylindrical coordinates; the assumption for *small meniscus slope*, $(\mathrm{d}z/\mathrm{d}r)^2 << 1$, has been used; K_0 is the modified Bessel function of the second kind and zero order;[87–89] q is the inverse capillary length; γ is the liquid/fluid interfacial tension; $\Delta\rho$ is the difference between the densities of the lower liquid and the upper fluid; g is the acceleration due to gravity; the multiplier Q is given by the expressions:

$$Q = \pm r_{\mathrm{c}} \sin\psi_{\mathrm{c}}, \qquad \sin\psi_{\mathrm{c}} \approx \tan\psi_{\mathrm{c}} = \left(\mathrm{d}\zeta / \mathrm{d}r\right)_{r=r_{\mathrm{c}}}. \tag{15.2}$$

Here, r_{c} is the radius of the three-phase contact line on the particle surface, and ψ_{c} is the meniscus-slope angle at this contact line; the assumption for small meniscus slope (which is always fulfilled for small particles, $r_{\mathrm{c}} << q^{-1}$) has been used again. The sign (plus or minus) in the definition of Q depends on whether the meniscus around the particle is convex or concave, and on the specific choice of the coordinate system.

An approximate, but numerically very accurate formula for the interaction energy due to the flotation capillary force (Figure 15.1a) can be obtained by using the Nicolson's superposition approximation.[1] For this goal, the motion of particle 2 toward particle 1 can be considered as sliding of particle 2 (under the action of its weight) over the meniscus created by particle 1. In this way, we can derive:[1,3,8,9]

$$\Delta W = -2\pi\gamma Q_1 Q_2 K_0(qL). \tag{15.3}$$

Here, ΔW is the capillary interaction energy; L is the center-to-center distance between the two particles;

$$Q_1 = \pm r_1 \sin\psi_1, \qquad Q_2 = \pm r_2 \sin\psi_2, \tag{15.4}$$

where r_1 and r_2 are the radii of the three-phase contact lines on particles 1 and 2; and ψ_1 and ψ_2 are the respective meniscus-slope angles (Figure 15.1a); the sign of Q_1 and Q_2 (plus or minus) is as in Equation 15.2. The minus sign in Equation 15.3 means that the capillary interaction corresponds to attraction. Furthermore, the force of capillary interaction is $F = -\mathrm{d}\Delta W/\mathrm{d}L$. Differentiating Equation 15.3, we obtain:

$$F = -2\pi\gamma Q_1 Q_2 q K_1(qL), \tag{15.5}$$

where K_1 is the modified Bessel function of the second kind and first order.[87–89] For small qL, we have $K_1(qL) \approx 1/(qL)$, and then Equation 15.5 acquires the form:

$$F = -2\pi\gamma \frac{Q_1 Q_2}{L} \quad \text{for} \quad qL << 1. \tag{15.6}$$

Equation 15.6 looks like a two-dimensional analog of the Coulomb's law of electricity, and for this reason the quantities Q_1 and Q_2 have been called *capillary charges*.[6,7] This analogy between capillary and electric forces has been further extended by introducing "capillary multipoles" as analogs of the electric multipoles;[10,54–56] see Section 15.2.2.

The "capillary charge" for floating particles can be estimated from the expression[3,6,9]

$$Q_i \approx \tfrac{1}{6} q^2 R_i^3 \left(2 - 4D_i + 3\cos\alpha_i - \cos^3\alpha_i\right), \quad (i = 1,2), \tag{15.7}$$

where $D_i = (\rho_i - \rho_{II})/(\rho_I - \rho_{II})$, ρ_i, ρ_I and ρ_{II} are the mass densities of the particle, lower and upper fluid phases, respectively. Equation 15.7 allows one to calculate the capillary charge Q_i directly from the particle radius R_i and the central angle α_i (by definition, $\sin\alpha_i = r_i/R$).

Flotation capillary forces have been found to affect many processes and phenomena in the mesoworld, that is, for particle sizes between 1 μm and 1 mm; see, for example, Refs. 9, 37 and the references therein. For smaller particles, the effect of the gravitational field becomes negligible, but one could use electric field created by electrodes parallel to the interface.[90,91] In electric field, the adsorbed dielectric particles experience a force normal to the liquid interface if their dielectric constant is different from those of the two neighboring fluid phases.

15.2.2 Forces between Capillary Multipoles

As mentioned above, the weight of micrometer-sized and sub- micrometer floating particles is not sufficient to deform the fluid interface and to bring about capillary force between the particles. However, interfacial deformation appears if the contact line at the particle surface has *undulated* or *irregular* shape (Figure 15.1b). This may happen when the particle surface is rough, angular or heterogeneous. In such cases, the contact line sticks to edges or to boundaries between domains on the heterogeneous surface. The undulated contact line

induces undulations in the surrounding fluid interface.[9,46,54] Let $z = \zeta(x,y)$ be the equation describing the interfacial shape around such isolated particle. Using polar coordinates (r, φ) in the xy-plane, we can express the interfacial shape as a Fourier expansion:[10,54–56]

$$\zeta(r,\varphi) = \sum_{m=1}^{\infty} r^{-m} \left(A_m \cos m\varphi + B_m \sin m\varphi\right), \tag{15.8}$$

where r is the distance from the particle centre, A_m and B_m are coefficients. In analogy with electrostatics, Equation 15.8 can be interpreted as a multipole expansion. The terms with $m = 1, 2, 3, \ldots$, play the role of capillary "dipoles", "quadrupoles", "hexapoles", and so on.[10,54–56] Here, the term with $m = 0$ (capillary "charge") is missing because it is assumed that there is no axisymmetric contribution to the deformation (negligible particle weight). The dipolar term with $m = 1$ disappears because it is annihilated by a spontaneous rotation of the floating particle around a horizontal axis (unless the particle is fixed to a holder).[54] Therefore, for freely floating particles the leading term is the quadrupolar one, with $m = 2$. The interaction between capillary quadrupoles has been theoretically investigated.[54,55] This interaction is nonmonotonic: attractive at long distances, but repulsive at short distances. Expressions for the rheological properties (surface dilatational and shear elasticity and yield stress) of Langmuir monolayers from angular particles have been derived.[9,46,55,56] "Mesoscale" capillary multipoles have been experimentally realized by Bowden et al.,[47,48] by appropriate hydrophobization or hydrophilization of the sides of small floating plates. Interactions between capillary quadrupoles have been observed between floating particles, which have the shape of curved disks[49] and ellipsoids.[50-53]

As already mentioned, for multipoles the sign and magnitude of the capillary force depend on the mutual orientation of the particle. For that reason, particles-quadrupoles ($m = 2$) will tend to assemble in a square lattice, whereas particles-hexapoles ($m = 3$) will preferably form a hexagonal lattice, with or without voids (Figure 15.2).[47,48] Another possibility is that the particles could form simple linear (chain) aggregates.[10,54] Such structures have been observed experimentally.[47–49, 92]

In Section 15.4 below, we review results about the forces due to capillary multipoles and give general analytical expressions for calculating these forces based on a recently developed theoretical approach.[93]

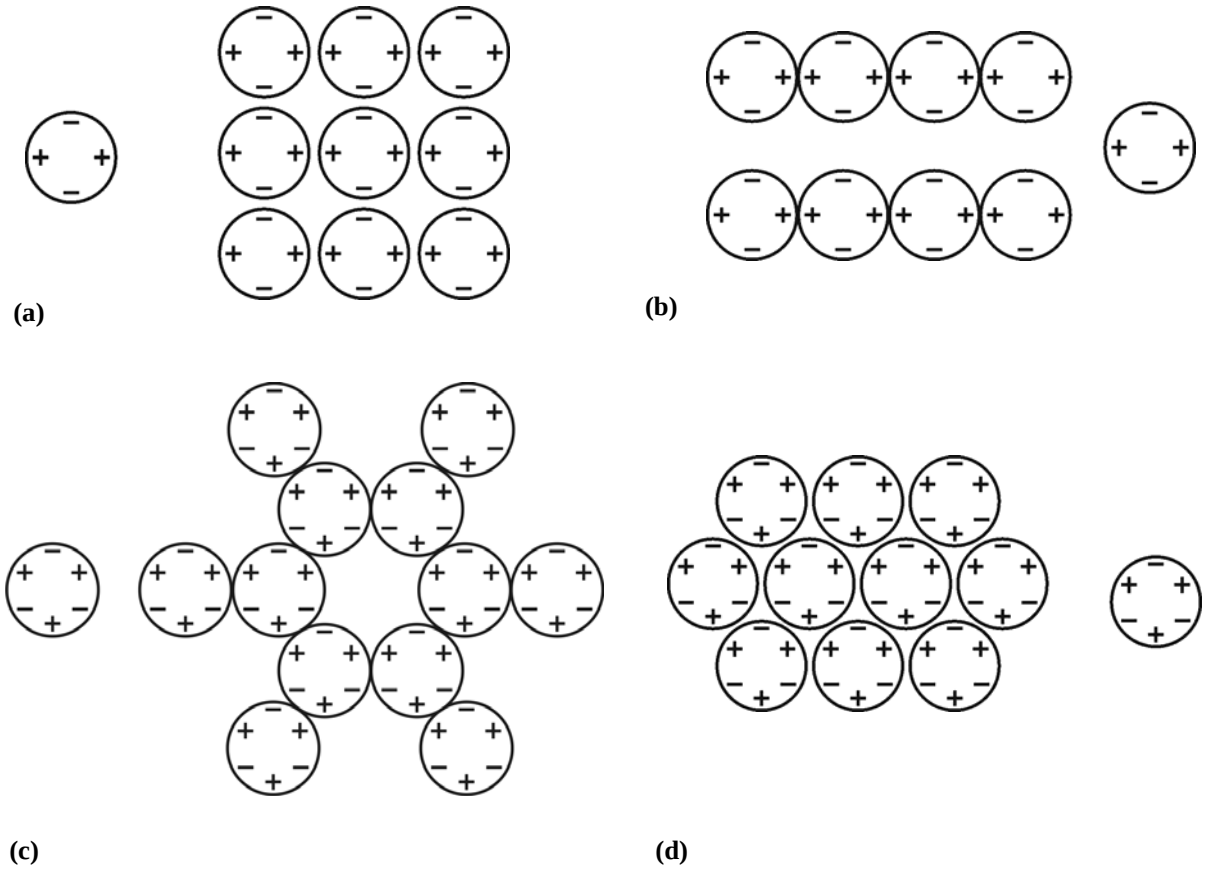

FIGURE 15.2 Two-dimensional arrays formed by capillary quadrupoles ($m = 2$) and hexapoles ($m = 3$). The quadrupoles form (a) tetragonal close-packed array or (b) linear aggregates. The hexapoles could form (c) hexagonal array with voids or (d) close-packed hexagonal array.[47–49, 92] The signs "+" and "–" denote, respectively, positive and negative "capillary charges", that is convex and concave local deviations of the meniscus shape from planarity at the contact line. In contrast with the electric charges, two similar capillary charges attract each other, while the interaction between opposite capillary charges is repulsive.[54–56]

15.2.3 Electric-Field-Induced Capillary Forces

Not only the gravitational field (Figure 15.1a), but also the electric field can induce interfacial deformations around an adsorbed particle, if this particle is electrically charged (Figure 15.1c). The overlap of the interfacial deformations around such two charged particles gives rise to electric-field-induced capillary force,[57] which has been termed for brevity *electrocapillary force*.[94] Being aware of the physical difference between the adsorption of molecules and particles, which is related to the great differences between their adsorption/desorption energies,[95] here and hereafter we are using also the term "adsorbed particle" as a substitute for "particle attached to an interface".

Let us consider a particle from a dielectric material, which is adsorbed at the boundary between water and a *nonpolar fluid*, for example, oil or air (Figure 15.1c). As a rule, such a particle bears surface electric charges, the absence of such charges being exclusion. Charges located near the boundary between two phases of different dielectric constants experience image-charge forces.[96–98] Because of that, *electrodipping force*, F_{ED}, is acting on each particle in direction toward the phase of greater dielectric constant,[58] in our case – toward water (Figure 15.1c).

At equilibrium, the electrodipping force is counterbalanced by the interfacial tension force: $F_{ED} = 2\pi r_c \gamma \sin\psi_c$, where γ is the interfacial tension; r_c is the radius of the contact line on the particle surface and ψ_c is the meniscus slope angle at the contact line (Figure 15.3). Consequently, F_{ED} can be determined from the experimental values of r_c, γ, and ψ_c. This approach was used to obtain the values of F_{ED} for silanized glass particles of radii 200–300 μm from photographs of these particles at an oil-water or air-water interface (Figure 15.4). F_{ED} was found to be much greater than the gravitational force acting on the particles.[58]

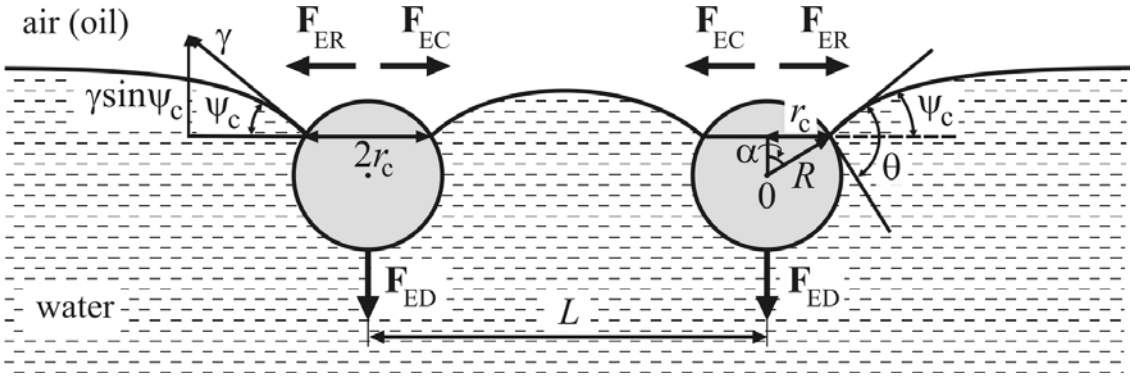

FIGURE 15.3 Sketch of two electrically charged particles attached to an oil-water interface. F_{ED} is the electrodipping force, due to the image-charge effect, that pushes the particles into water and deforms the fluid interface around the particles. F_{ER} is the direct electric repulsion between the two like-charged particles. F_{EC} is the electrocapillary attraction, related to deformations in the fluid interface created by the electric field.

Figure 15.4 compares the profiles of the liquid menisci around a noncharged particle and a charged particle. The particles represent hydrophobized glass spheres of density ρ_p = 2.5 g/cm^3. The oil phase is purified soybean oil of density ρ_{oil} = 0.92 g/cm^3. The oil-water interfacial tension is γ = 30.5 mN/m. The calculated surface tension force, $2\pi r_c \gamma \sin\psi_c$, which counterbalances the gravitational force (particle weight minus the Archimedes force) corresponds to meniscus slope angle ψ_c = 1.5°, and the deformation of the liquid interface

caused by the particle is hardly visible (Figure 15.4a). In contrast, for the charged particle (Figure 15.4b), the meniscus slope angle is much greater, $\psi_c = 26°$. This is due to the fact that the electrodipping force, F_{ED}, which pushes the particle toward the water phase, has to be counterbalanced by the interfacial-tension force, $2\pi r_c \gamma \sin\psi_c$. Experimentally, it has been found that the angle ψ_c is insensitive to the concentration of NaCl in the aqueous phase, which means that (in the investigated case) the electrodipping force is due to charges situated at the particle-oil interface.[58,60] With similar particles, the magnitude of F_{ED} at the air-water interface was found to be about six times smaller than at the oil-water interface.[58]

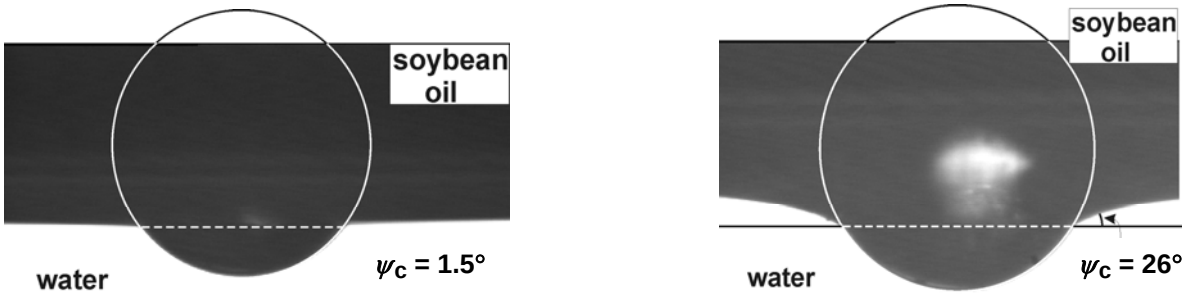

(a) uncharged particle **(b) charged particle**

FIGURE 15.4 Side-view photographs of hydrophobized spherical glass particles at the boundary water/soybean oil (no added surfactants). (a) Uncharged particle of radius $R = 235$ μm: the meniscus slope angle due to gravity is relatively small, $\psi_c = 1.5°$. (b) Electrically-charged particle of radius $R = 274$ μm: the experimental meniscus slope angle is $\psi_c = 26°$ owing to the electrodipping force, F_{ED} (see Figure 15.3). If this force were missing, the gravitational slope angle of this particle would be only $\psi_c = 1.9°$.

In the case when the electrostatic interactions are dominated by the field of charges situated at the particle/*nonpolar-fluid* interface, F_{ED} can be calculated from the expression:[59,60]

$$F_{ED} = (4\pi/\varepsilon_n)(\sigma_{pn}R)^2(1 - \cos\alpha)f(\theta,\varepsilon_{pn}). \qquad (15.9)$$

Here, R is the particle radius; ε_n is the dielectric constant of the nonpolar fluid (oil, air); σ_{pn} is the surface charge density at the boundary particle–nonpolar fluid; $\varepsilon_{pn} = \varepsilon_p/\varepsilon_n$ is the ratio of the respective two dielectric constants; α is a central angle; $\theta = \alpha + \psi_c$ is the contact angle (see Figure 15.3). On the basis of the solution of the electrostatic boundary problem, we can accurately calculate the dimensionless function $f(\theta,\varepsilon_{pn})$ by means of the relation $f(\theta,\varepsilon_{pn}) = f_R(\theta,\varepsilon_{pn})/(1 - \cos\theta)$, where the function $f_R(\theta,\varepsilon_{pn})$ is tabulated: see Table 3 in Ref. 59.

The tabulated values can be used for a convenient computer calculation of $f_R(\theta,\varepsilon_{pn})$ with the help of a four-point interpolation formula, Equation D.1 in Ref. 59. From the experimental F_{ED} and Equation 15.9, we could determine the surface charge density, σ_{pn}, at the particle-oil and particle-air interface. Values of σ_{pn} in the range from 20 to 70 $\mu C/m^2$ have been obtained.[58,60,63,64,99,100]

In the other limiting case, when the electrostatic interactions are dominated by the field of surface charges of density σ_{pw} situated at the particle/*water* interface, F_{ED} can be calculated from the expression:[58]

$$F_{ED} = \frac{16\pi r_c^2 kTC}{\kappa R}\left[\cosh\left(\frac{e\varphi_{pw}}{2kT}\right)-1\right], \quad \sigma_{pw} = \frac{4eC}{\kappa}\sinh\left(\frac{e\varphi_{pw}}{2kT}\right) \quad (\kappa R >> 1). \quad (15.10)$$

Here, k is the Boltzmann constant; T is the temperature; C is the bulk concentration of 1:1 electrolyte; e is the elementary electric charge; $\kappa = (2e^2C/\varepsilon_0\varepsilon_w kT)^{1/2}$ is the Debye screening parameter; ε_0 is the dielectric constant of vacuum; and φ_{pw} is the electric potential at the particle/water boundary with respect to the bulk water phase; Equation 15.10 is valid for $\kappa R >> 1$. Eliminating φ_{pw}, we can bring Equation 15.10 in the form:

$$F_{ED} = \frac{16\pi r_c^2 kTC}{\kappa R}\left\{\left[1+\left(\frac{\kappa\sigma_{pw}}{4eC}\right)^2\right]^{1/2}-1\right\} \quad (\kappa R >> 1). \quad (15.11)$$

For not so great σ_{pw}, the square root in Equation 15.11 can be expanded in series. In such a case, Equation 15.11 predicts that F_{ED} should decay with the rise of the electrolyte concentration, C. Correspondingly, the depth of the meniscus around the particle (like that in Figure 15.4b) should diminish, which would lead to a greater surface mobility of the particle.[101,102]

Two like-charged particles at a liquid interface (Figure 15.1c) experience both *direct electric repulsion*, F_{ER},[62–64] and *electrocapillary force*,[57] F_{EC}. Note that F_{ED} acts on each individual particle, while F_{ER} and F_{EC} are interaction forces between two (or more) particles (Figure 15.3).

For a particle in isolation, the charges at the particle/nonpolar-fluid interface create electric field in the nonpolar fluid (oil, air) that asymptotically resembles the electric field of a

dipole, because of the image-charge effect (Figure 15.5). This field practically does not penetrate into the water phase, because it is reflected by the oil-water boundary owing to the relatively large dielectric constant of water. For a single particle, the respective electrostatic problem has been solved.[58,59] The asymptotic behavior of the force of *direct electric repulsion* between two such particles-dipoles (Figure 15.5) is:[59,62]

$$F_{\mathrm{ER}} = \frac{3p_{\mathrm{d}}^2}{2\varepsilon_{\mathrm{n}} L^4} \qquad (L/r_{\mathrm{c}} >> 1). \tag{15.12}$$

L is the center-to-center distance between the two particles; the quantity

$$p_{\mathrm{d}} = 4\pi\sigma_{\mathrm{pn}} D R^3 \sin^3\alpha \tag{15.13}$$

is the effective particle dipole moment;[59] R is the particle radius, α is central angle (Figure 15.3), and σ_{pn} is the electric charge density at the particle/nonpolar-fluid interface; $D = D(\alpha,\varepsilon_{\mathrm{pn}})$ is a known dimensionless function, which can be calculated by means of Table 1 and Equation D.1 in Ref. 59; $\varepsilon_{\mathrm{pn}} \equiv \varepsilon_{\mathrm{p}}/\varepsilon_{\mathrm{n}}$ is the ratio of the dielectric constants of the two phases. Equation 15.12 shows that F_{ER} asymptotically decays as $1/L^4$ like the force between two-point dipoles. However, at shorter distances, the finite size of the particle is expected to lead to a Coulombic repulsion, $F_{\mathrm{ER}} \sim 1/L^2$.[62–64]

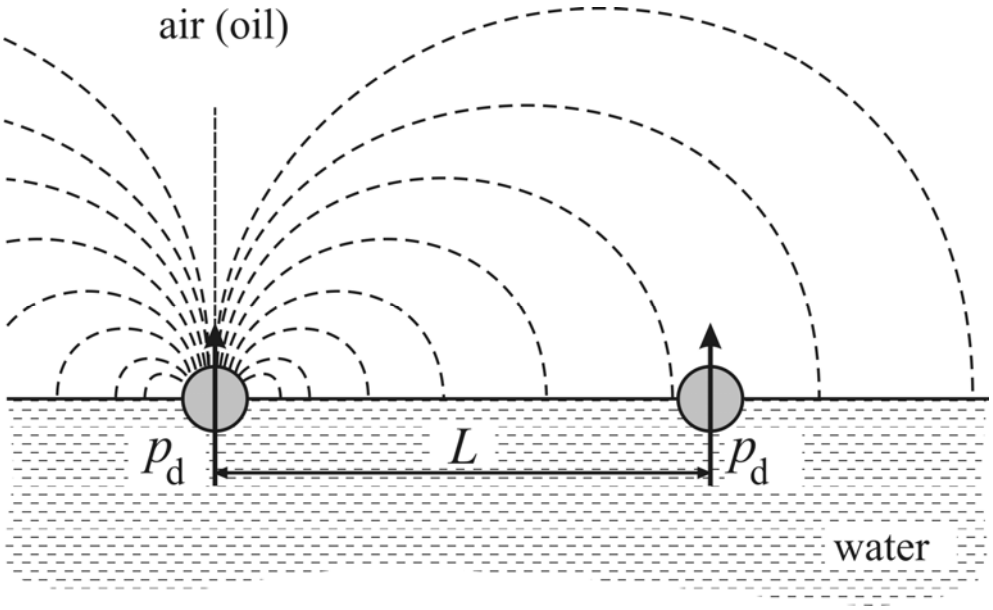

FIGURE 5 Two particles attached to the boundary water–nonpolar fluid and separated at a center-to-center distance L. In the nonpolar fluid (oil, air), the electric field of each separate particle is asymptotically identical to the field of a dipole of moment p_{d}. This field is created by charges at the particle/nonpolar-fluid interface.

Equation 15.13 is derived for the case, when the surface charges are located at the particle/nonpolar-fluid interface. In this case, the total interaction force between the two particles (Figure 15.1c), of both electric and capillary origin, is:[103]

$$F = F_{\mathrm{ER}} + F_{\mathrm{EC}} = \frac{3p_{\mathrm{d}}^2}{2\varepsilon_{\mathrm{n}} L^4}[1 - \frac{2\delta}{5} + O(\frac{r_{\mathrm{c}}}{L})^2] \qquad (L/r_{\mathrm{c}} >> 1), \tag{15.14}$$

$$\delta \equiv \frac{p_{\mathrm{d}}^2}{32\pi\gamma\varepsilon_{\mathrm{n}} r_{\mathrm{c}}^5} = \tan\psi_{\mathrm{c}}\,. \tag{15.15}$$

In view of Equation 15.12, the force of electrocapillary attraction is:[103]

$$F_{\mathrm{EC}} = -\frac{3p_{\mathrm{d}}^2}{5\varepsilon_{\mathrm{n}} L^4}[\delta + O(\frac{r_{\mathrm{c}}}{L})^2] \qquad (L/r_{\mathrm{c}} >> 1). \tag{15.16}$$

$\delta = \tan\psi_{\mathrm{c}}$ can be either measured experimentally from photographs like Figure 15.4, or calculated from Equation 15.15. Outline of the derivation of Equations 15.14 through 15.16 is given in Section 15.5; details can be found in Ref. 103.

Because we consider the case of small meniscus slope, $\delta = \tan\psi_{\mathrm{c}} < 1$, the term $2\delta/5$ in Equation 15.14 is always smaller than 1. This means that always $|F_{\mathrm{EC}}| < F_{\mathrm{ER}}$, that is, the electrocapillary attraction is always weaker than the direct electric repulsion, at least in the asymptotic region of long distances, $L/r_{\mathrm{c}} >> 1$. In other words, in the considered case, of electric charges, which are uniformly distributed over the particle/nonpolar-fluid interface, the electrocapillary attraction is weaker than the direct electric repulsion,[103] both of them asymptotically decaying as $1/L^4$; see Equations 15.12 and 15.16.

Note, however, that the situation changes if the electric charges are not uniformly distributed over the particle/nonpolar-fluid interface. In Ref. 104 and Section 15.6 it is demonstrated that in such a case it is possible to have capillary attraction that is stronger and has longer range than the electrostatic repulsion, in agreement with the experiment.[61]

15.2.4 Capillary Immersion Forces

Capillary interaction appears also when the particles (instead of being freely floating) are partially immersed (confined) in a liquid film; this is the *immersion* capillary force (Figure 15.1d–f). The deformation of the liquid surface in this case is related to the wetting properties of the particle surface, that is, to the position of the contact line and the magnitude of the contact angle, rather than to gravity. The immersion capillary force, resulting from the overlap of such interfacial deformations, can be large enough to cause 2D aggregation and ordering of small colloidal particles,[4,7–9] as observed in many experiments. In particular, colloidal particles and protein macromolecules confined in liquid films exhibit attraction and form clusters and larger ordered domains (2D arrays).[8–13,25,26] Capillary immersion forces appear also between partially immersed bodies like vertical plates,[2] vertical cylinders (rods), and so on.[4,5,7–9,105–109]

For the first time, the capillary forces between two vertical cylinders and between two spheres partially immersed in a liquid layer were theoretically studied in Ref. 4. A general expression for the interaction energy has been used, which includes contributions from the energy of particle wetting, the gravitational energy, and the energy of increase of the meniscus area due to the deformation caused by the particles; this expression is valid for both floating and confined particles. Expressions and numerical results for the energy and force of interaction have been obtained for the case of small slope of the deformed meniscus; this case has a physical and practical importance because it corresponds to the usual experimental situation with small particles. The theory has been extended also to particles entrapped in *thin* films, for which the disjoining pressure effect, rather than gravity, keeps the non-deformed surface planar.[7]

In the particular case, when the particle radii are equal, $R_1 = R_2 = R$ and $r_k << L << q^{-1}$, from Equation 15.5 we can derive:[7–9]

$$F \propto (R^6/\gamma) K_1(qL) \quad \text{for flotation force,}$$

$$F \propto \gamma R^2 K_1(qL) \qquad \text{for immersion force.} \tag{15.17}$$

The above expression for the immersion force follows from Equation 15.4, whereas that for the flotation force follows from Equation 15.7. Equation 15.17 shows that the flotation force decreases, while the immersion force increases, when the interfacial tension γ increases. Besides, the flotation force decreases much strongly with the decrease of particle size

($F \propto R^6$) than the immersion force ($F \propto R^2$). Thus, the flotation force becomes negligible for $R < 5–10$ μm, whereas the immersion force can be significant even for $R \approx 3$ nm. As already mentioned, the latter force is one of the main factors causing the self-assembly of small colloidal particles, viruses, and protein macromolecules confined in thin liquid films; see Refs. 7–9 for details.

The theory was verified in measurements of capillary immersion forces by Velev et al.[106] for vertical cylinders by piezo-transduser balance and by Dushkin et al.[107-109] for spherical particles and cylinders attached to a sensitive torsion balance. Recently, di Leonardo et al.[110] directly measured capillary immersion forces between two colloidal spheres located in a liquid film by means of laser optical tweezers. The capillary attraction between particles confined in *free* liquid films has been found to produce spontaneous formation and growth of densely packed particle monolayers in the film.[65,111–114]

The immersion capillary force can be also operative between particles captured in a *spherical* (rather than planar) thin liquid film or lipid vesicle. In this case the "capillary charge" characterizes the local deviation of the meniscus shape from sphere.[9,115]

15.2.5 Capillary Forces in the Case of Finite Menisci

Equation 15.1, which describes a meniscus decaying at infinity, is not valid for all physically possible cases. For example, when the particle diameter is much greater than the thickness of the surrounding liquid film (Figure 15.1e), the meniscus profile near an isolated particle, $z = \zeta(r)$, obeys the Laplace equation of capillarity in the form:

$$\frac{\gamma}{r}\frac{\mathrm{d}}{\mathrm{d}r}\left(r\frac{\mathrm{d}\zeta}{\mathrm{d}r}\right) = P_{\mathrm{c}} = \text{const.} \tag{15.18}$$

The capillary pressure, P_{c}, is the pressure jump across the meniscus. For particle diameters between 1 μm and 1 mm, P_{c} is constant because the effects of the gravitational hydrostatic pressure and molecular disjoining pressure are both negligible. Then, the solution of Equation 15.18 is:[89]

$$\zeta(r) = A + B\ln r + (P_{\mathrm{c}}/4\gamma)r^2. \tag{15.19}$$

Hence, in the considered case the Laplace equation has no axisymmetric solution that is finite at infinity ($r \to \infty$). The latter fact implies that the meniscus around the particle must end at a *peripheral contact line* (of radius r_p), out of which the film is plane-parallel ($\zeta \equiv 0$), see Figure 15.1e. In other words, we are dealing with a *finite* meniscus. In this case, the overlap of the menisci, and the interaction between the particles, begins when they come at a distance $L < 2r_p$ from each other. This type of interaction is obviously different from that described by Equation 15.3. The respective capillary force can be calculated from the derived integral expressions by means of numerical integration.[116,117]

Velikov et al.[118] observed a strong attraction between latex particles of diameter $2R \approx 7$ μm entrapped in a foam film whose thickness was at least 100 times smaller. Danov et al.[116,117] described analogous observations with micrometer-sized latex spheres encapsulated within the bilamellar membrane of a giant lipid vesicle. The latter experiments, based on optical manipulation and dynamometry (optical tweezers), neatly reveal the film deformation caused by the particles and the related attraction between them. Basic characteristics of the meniscus were deduced from photographs of the vesicle-particle system, and the experimental capillary force profile is found from the analysis of the trajectories of pairs of particles, which are moving toward each other under the action of the capillary attraction. The computed profile quantitatively fits to the experimental data, with a single adjustable parameter, the bilayer tension. In general, the capillary force was found to be strong enough to cause aggregation of the confined colloidal particles.[116,117]

15.2.6 Interactions between Inclusions in Lipid Membranes

A bilayer lipid membrane cannot be simply modeled as a thin liquid film because the hydrocarbon chain interior of the membrane exhibits elastic behavior when its thickness is varied. The hybrid mechanical behavior of a lipid bilayer (neither liquid nor bulk elastic body) can be described by means of a mechanical model, which treats the membrane as a special elastic film (the hydrocarbon chain interior) sandwiched between two Gibbs dividing surfaces (the surface polar head group layers of the membrane). This *sandwich model*[9,43,44] involves mechanical parameters such as the shear elastic modulus of the hydrocarbon chain interior, the bilayer surface tension, stretching (Gibbs) elasticity, surface bending moment and

curvature elastic moduli. A mechanical analysis of the bilayer deformations enables one to derive expressions for the total stretching, bending and torsion (Gaussian) moduli of the membrane as a whole in terms of the aforementioned mechanical parameters of the model.

Inclusions in a lipid membrane (like membrane proteins) cause deformations in the bilayer surfaces accompanied by displacements in the membrane hydrocarbon interior (Figure 15.1f). In the case of not-too-low membrane surface tension the shape of the membrane surfaces is governed by an analog of the Laplace equation of capillarity. The theory of the capillary immersion forces,[4,5] was extended and applied to describe the interactions between two inclusions in a lipid membrane.[9,43,44] The range of the obtained attractive force turns out to be of the order of several inclusion radii. The magnitude of interaction is estimated to be sufficient to bring about aggregation of the inclusions. The theoretical predictions are in agreement with the experimental observations, although additional data about the membrane mechanical parameters are needed to achieve an actually quantitative comparison.

As an example, Figure 15.1f shows two integral membrane proteins incorporated in a lipid membrane. The width of the hydrophobic belt of the protein is greater than the thickness, h, of the hydrophobic interior of the nondisturbed membrane. For this reason, a mismatch, h_c, appears (Figure 15.1f) which leads to deformations in the membrane near each inclusion. The overlap of the deformations around two inclusions gives rise to attraction between them, which is analogous to the capillary immersion force. The respective interaction energy is given by the expression:[43]

$$\Delta W(L) = 2\pi\gamma\, q r_c h_c^2 \left[\frac{K_1(qr_c) - \frac{1}{2} qr_c K_0(qL)}{K_0(qr_c) + K_0(qL)} - \frac{K_1(qr_c)}{K_0(qr_c)} \right]. \qquad (15.20)$$

For a bilayer lipid membrane, we have $q \approx [4\lambda/(h\gamma)]^{1/2}$, where λ is the shear elastic modulus in the hydrocarbon chain zone and γ is the membrane "surface tension"; for details, see Refs. 43, 44, and chapter 10 in Ref. 9. Note that the interaction energy, as given by Equation 15.20, is proportional to h_c^2, that is, to the squared mismatch between the hydrophobic zones of the inclusion and bilayer. This interaction is one of the reasons for the dynamics and aggregation of membrane proteins in biomembranes.[119–129]

15.3 General Expressions for the Capillary Force between Particles at a Liquid Interface

15.3.1 Obtaining the Capillary Force by Integration over the Midplane

Here, we give an outline of the results in Ref. 93, where a general expression is derived for the lateral capillary force between two particles. This expression is applicable to floating axisymmetric particles (Figure 15.1a); to capillary multipoles of different orders (Figure 15.1b), and to electrically charged particles (Figure 15.1c). For this goal, we consider two spherical particles separated at a center-to-center distance L, like those in Figures 15.1a–c. The liquid interface is assumed to be planar in the absence of adsorbed particles. The xy-plane of the coordinate system is chosen to coincide with the nondisturbed liquid interface. The x-axis passes through the vertical axes of the two particles, and the yz-plane is located in the middle between the two particles. The meniscus shape is given by the equation $z = \zeta(x,y)$. The lower and upper fluid phases are denoted, respectively, as "phase a" and "phase b" (Figure 15.6).

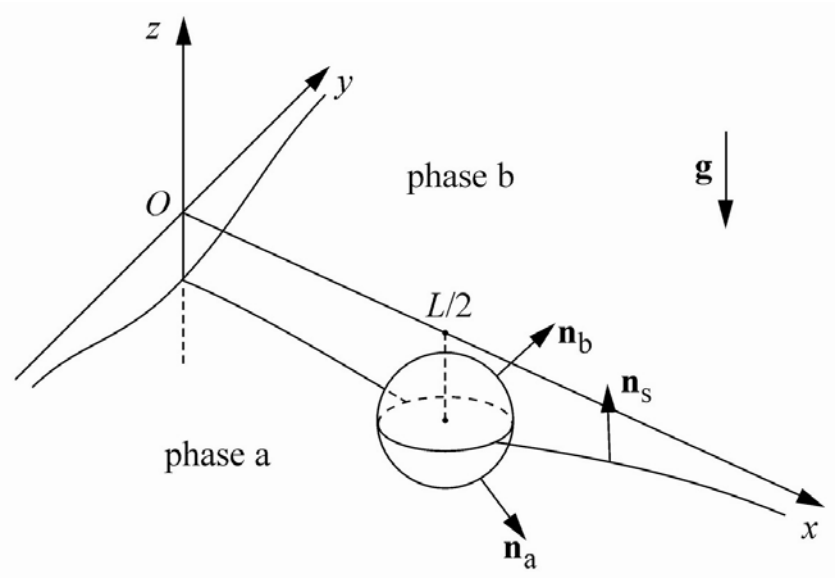

FIGURE 15.6 Sketch of a particle that is attached to the interface between phases "a" and "b". The vertical yz-plane represents the midplane between two particles (like the pairs shown in Figure 15.1). The horizontal xy-plane coincides with the unperturbed liquid interface far from the particles. The x-axis is parallel to the force of interaction between the two particles; $\mathbf{n}_a$, $\mathbf{n}_b$ and $\mathbf{n}_s$ are unit vector fields normal to the interfaces particle/phase a; particle/phase b, and to the liquid interface, respectively.

At hydrostatic equilibrium, the divergence of the pressure tensor in the bulk phases is equal to zero:[130]

$$\nabla \cdot \mathbf{P}_\mathrm{a} = \mathbf{0} \quad \text{and} \quad \nabla \cdot \mathbf{P}_\mathrm{b} = \mathbf{0}, \tag{15.21}$$

where ∇ denotes the del operator; $\mathbf{P}_\mathrm{a}$ and $\mathbf{P}_\mathrm{b}$ are the pressure tensors in the phases "a" and "b". Likewise, at equilibrium the shape of the liquid interface obeys the Laplace equation of capillarity:

$$2H\gamma = \mathbf{n}_\mathrm{s} \cdot (\mathbf{P}_\mathrm{b} - \mathbf{P}_\mathrm{a}) \cdot \mathbf{n}_\mathrm{s} \quad \text{at} \quad z = \zeta, \tag{15.22}$$

where H is the mean curvature of the surface $z = \zeta(x,y)$; $\mathbf{n}_\mathrm{s}$ is the running unit normal to this interface directed toward phase "b"; as usual, γ is the interfacial tension.

Let us consider the right-hand-side particle (Figure 15.6). The force acting on this particle is:[5]

$$\mathbf{F} = \mathbf{F}^{(\mathrm{p})} + \mathbf{F}^{(\gamma)}, \tag{15.23}$$

where the force $\mathbf{F}^{(\mathrm{p})}$ represents the integral of pressure tensor over the particle surface and $\mathbf{F}^{(\gamma)}$ is the integral of the interfacial tension, considered as a vector, over the contact line, C:

$$\mathbf{F}^{(\mathrm{p})} = -\int_{S_\mathrm{a}} \mathrm{d}S\, \mathbf{n}_\mathrm{a} \cdot \mathbf{P}_\mathrm{a} - \int_{S_\mathrm{b}} \mathrm{d}S\, \mathbf{n}_\mathrm{b} \cdot \mathbf{P}_\mathrm{b}, \qquad \mathbf{F}^{(\gamma)} = \int_C \mathrm{d}l\, \mathbf{m}\gamma. \tag{15.24}$$

Here, S_a and S_b are the portions of the particle surface that make contact with phases "a" and "b", respectively; $\mathbf{n}_\mathrm{a}$ and $\mathbf{n}_\mathrm{b}$ are outer unit normal fields with respect to the particle (Figure 15.6); $\mathrm{d}l$ is the scalar linear element of the contact line C; $\mathbf{m}$ is the outward pointing unit normal field having the direction of the surface tension at the contact line, that is, normal to C and tangential to the liquid interface.

To calculate $\mathbf{F}^{(\gamma)}$, we will use the fact that the Laplace equation, Equation 15.22, is the normal projection (along $\mathbf{n}_\mathrm{s}$) of a more general equation (see, e.g., Ref. 9):

$$\nabla_\mathrm{s} \cdot (\gamma \mathbf{U}_\mathrm{s}) = \mathbf{n}_\mathrm{s} \cdot (\mathbf{P}_\mathrm{b} - \mathbf{P}_\mathrm{a}) \quad \text{at} \quad z = \zeta, \tag{15.25}$$

where ∇_s and $\mathbf{U}_\mathrm{s}$ are the del operator and the unit tensor of the surface $z = \zeta(x,y)$. Following the approach proposed in Ref. 106, we consider a rectangle ABMN situated in the xy-plane as shown in Figure 15.7. Next, we integrate Equation 15.25 over the surface S_ABMN, which represents the vertical projection of the rectangle ABMN on the interface $z = \zeta(x,y)$:

$$\int_{S_\mathrm{ABMN}} \mathrm{d}S \mathbf{n}_\mathrm{s} \cdot (\mathbf{P}_\mathrm{b} - \mathbf{P}_\mathrm{a}) = \int_{S_\mathrm{ABMN}} \mathrm{d}S\, \nabla_\mathrm{s} \cdot (\gamma \mathbf{U}_\mathrm{s}) = \int_{C_\mathrm{ABMN}} \mathrm{d}l\, \mathbf{m}\gamma - \mathbf{F}^{(\gamma)}, \tag{15.26}$$

where the contour C_{ABMN} is the periphery of S_{ABMN} and we have used the 2D divergence theorem.[9,131] Using the fact that the meniscus $z = \zeta(x,y)$ decays at infinity, we assume that the points A, B, M and N are located far from the particle, and then the x-projection of Equation 15.26 acquires the form:

$$F_x^{(\gamma)} \equiv \mathbf{e}_x \cdot \mathbf{F}^{(\gamma)} = \int\limits_{C_{\mathrm{AB}} \cup C_{\mathrm{MN}}} \mathrm{d}l \quad (\mathbf{e}_x \cdot \mathbf{m})\gamma - \int\limits_{S_{\mathrm{ABMN}}} \mathrm{d}S \mathbf{n}_{\mathrm{s}} \cdot (\mathbf{P}_{\mathrm{b}} - \mathbf{P}_{\mathrm{a}}) \cdot \mathbf{e}_x \,. \tag{15.27}$$

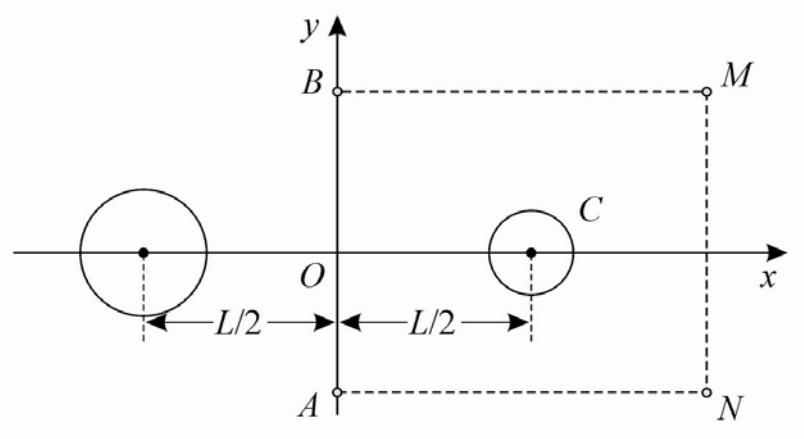

FIGURE 15.7 Integration domains for calculating the interaction force between two particles (details in the text). The projections of the contact lines on the particle surfaces are presented by two circles, but they could be arbitrary closed contours. The x-axis is parallel to the force of interaction between the two particles.

Next, we consider a right prism built on the rectangle ABMN with lower and upper bases situated deeply in the interior of the phases "a" and "b". In view of Equation 15.21, we have:

$$0 = \int\limits_{V^{(\mathrm{a})}} \mathrm{d}V \nabla \cdot \mathbf{P}_{\mathrm{a}} = \oint\limits_{\partial V^{(\mathrm{a})}} \mathrm{d}\mathbf{S} \cdot \mathbf{P}_{\mathrm{a}} \ , \tag{15.28}$$

where $V^{(\mathrm{a})}$ is the portion of the aforementioned vertical prism that is located in the phase "a", and $\partial V^{(\mathrm{a})}$ is the surface of $V^{(\mathrm{a})}$; $\mathrm{d}\mathbf{S}$ is the respective outward pointing vectorial surface element. In view of the symmetry of the system, the x-projection of Equation 15.28 can be presented in the form:

$$0 = \mathbf{e}_x \cdot [\int\limits_{S_{\mathrm{ABMN}}} \mathrm{d}S \mathbf{n}_{\mathrm{s}} \cdot \mathbf{P}_{\mathrm{a}} + \int\limits_{S_{\mathrm{AB}}^{(\mathrm{a})}} \mathrm{d}\mathbf{S} \cdot \mathbf{P}_{\mathrm{a}} + \int\limits_{S_{\mathrm{MN}}^{(\mathrm{a})}} \mathrm{d}\mathbf{S} \cdot \mathbf{P}_{\mathrm{a}} - \int\limits_{S_{\mathrm{a}}} \mathrm{d}S \mathbf{n}_{\mathrm{a}} \cdot \mathbf{P}_{\mathrm{a}}] \,. \tag{15.29}$$

Here, $S_{\mathrm{AB}}^{(\mathrm{a})}$ and $S_{\mathrm{MN}}^{(\mathrm{a})}$ are the portions of the vertical planes passing through the segments AB and MN, which are in contact with the phase "a"; S_{a} is the same in Equation 15.24. Likewise, we derive a counterpart of Equation 15.29 for the phase "b":

$$0 = \mathbf{e}_x \cdot [- \int\limits_{S_{\mathrm{ABMN}}} \mathrm{d}S\, \mathbf{n}_{\mathrm{s}} \cdot \mathbf{P}_{\mathrm{b}} + \int\limits_{S_{\mathrm{AB}}^{(\mathrm{b})}} \mathrm{d}\mathbf{S} \cdot \mathbf{P}_{\mathrm{b}} + \int\limits_{S_{\mathrm{MN}}^{(\mathrm{b})}} \mathrm{d}\mathbf{S} \cdot \mathbf{P}_{\mathrm{b}} - \int\limits_{S_{\mathrm{b}}} \mathrm{d}S\, \mathbf{n}_{\mathrm{b}} \cdot \mathbf{P}_{\mathrm{b}}]\,. \tag{15.30}$$

In view of Equations 15.24, we sum Equations 15.29 and 15.30, and obtain:

$$F_x^{(\mathrm{p})} \equiv \mathbf{e}_x \cdot \mathbf{F}^{(\mathrm{p})} = \mathbf{e}_x \cdot [\int\limits_{S_{\mathrm{ABMN}}} \mathrm{d}\mathbf{S} \cdot (\mathbf{P}_{\mathrm{b}} - \mathbf{P}_{\mathrm{a}}) - \int\limits_{S_{\mathrm{AB}}} \mathrm{d}\mathbf{S} \cdot \mathbf{P} - \int\limits_{S_{\mathrm{MN}}} \mathrm{d}\mathbf{S} \cdot \mathbf{P}]\,, \tag{15.31}$$

where $S_{\mathrm{AB}} = S_{\mathrm{AB}}^{(\mathrm{a})} \cup S_{\mathrm{AB}}^{(\mathrm{b})}$ and $S_{\mathrm{MN}} = S_{\mathrm{MN}}^{(\mathrm{a})} \cup S_{\mathrm{MN}}^{(\mathrm{b})}$ are stripes of vertical planes that are based on the segments AB and MN;

$$\mathbf{P} \equiv \mathbf{P}_{\mathrm{a}} \ \text{ for } z < \zeta, \ \text{ and } \ \mathbf{P} \equiv \mathbf{P}_{\mathrm{b}} \ \text{ for } z > \zeta\,. \tag{15.32}$$

Finally, we sum up Equations 15.27 and 15.31; the integrals over S_{ABMN} cancel each other, and we obtain the following expression for the total force acting on the right-hand side particle (Figure 15.6):

$$F_x \equiv F_x^{(\gamma)} + F_x^{(\mathrm{p})} = \int\limits_{C_{\mathrm{AB}} \cup C_{\mathrm{MN}}} \mathrm{d}l \quad (\mathbf{e}_x \cdot \mathbf{m})\gamma - \int\limits_{S_{\mathrm{AB}} \cup S_{\mathrm{MN}}} \mathrm{d}\mathbf{S} \cdot \mathbf{P} \cdot \mathbf{e}_x\,. \tag{15.33}$$

Let us denote the first and the second integral in the right-hand side of Equation 15.33 by $F_x^{(C)}$ and $F_x^{(S)}$, respectively. Because the segments AB and MN are perpendicular to the x-axis, and the points A, B, M and N (by definition) are located far away from the particle, we have:

$$F_x^{(C)} \equiv \int\limits_{C_{\mathrm{AB}} \cup C_{\mathrm{MN}}} \mathrm{d}l \quad (\mathbf{e}_x \cdot \mathbf{m})\gamma = \gamma \int\limits_{-\infty}^{\infty} \mathrm{d}y \{1 - [(1+\zeta_y^2)/(1+\zeta_x^2)]^{1/2}\}\big|_{x=0}\,, \tag{15.34}$$

where $\zeta_x \equiv \partial\zeta/\partial x$, $\zeta_y \equiv \partial\zeta/\partial y$ and γ is a constant. Likewise, we obtain:

$$F_x^{(S)} \equiv - \int\limits_{S_{\mathrm{AB}} \cup S_{\mathrm{MN}}} \mathrm{d}\mathbf{S} \cdot \mathbf{P} \cdot \mathbf{e}_x = \int\limits_{-\infty}^{\infty} \int\limits_{-\infty}^{\infty} \mathrm{d}y \mathrm{d}z\, \mathbf{e}_x \cdot \left(\mathbf{P}\big|_{x=0} - \mathbf{P}\big|_{x \to \infty}\right) \cdot \mathbf{e}_x\,. \tag{15.35}$$

In view of the definition of **P**, given by Equation 15.32, the above expression can be represented in the form:

$$F_x^{(S)} = \int_{-\infty}^{\infty} \mathrm{d}y [\int_{-\infty}^{\zeta} \mathrm{d}z\, \mathbf{e}_x \cdot \mathbf{P}_{\mathrm{a}0} \cdot \mathbf{e}_x - \int_{-\infty}^{0} \mathrm{d}z\, \mathbf{e}_x \cdot \mathbf{P}_{\mathrm{a}\infty} \cdot \mathbf{e}_x]$$

$$+ \int_{-\infty}^{\infty} \mathrm{d}y [\int_{\zeta}^{\infty} \mathrm{d}z\, \mathbf{e}_x \cdot \mathbf{P}_{\mathrm{b}0} \cdot \mathbf{e}_x - \int_{0}^{\infty} \mathrm{d}z\, \mathbf{e}_x \cdot \mathbf{P}_{\mathrm{b}\infty} \cdot \mathbf{e}_x], \qquad (15.36)$$

where the subscripts "0" and "∞" denote the values of the respective quantity at $x = 0$ and at $x \to \infty$, respectively.

In view of Equations 15.33 through 15.35, the total interaction force, F_x, can be expressed in two alternative forms:

$$F_x \equiv F_x^{(\mathrm{p})} + F_x^{(\gamma)} = F_x^{(S)} + F_x^{(C)}, \qquad (15.37)$$

where $F_x^{(\mathrm{p})}$ and $F_x^{(\gamma)}$ are integrals over the particle surface and contact line, whereas $F_x^{(S)}$ and $F_x^{(C)}$ are related to integrals over the surface and line on the midplane $x = 0$; see Figure 15.6. In other words, there are two equivalent approaches for calculation of F_x: (i) by integration over the particle surface[5] and (ii) by integration over the midplane.[106] Depending on the specific problem, we could use that approach, which is more convenient. In general, $F_x^{(\mathrm{p})} \neq F_x^{(S)}$ and $F_x^{(\gamma)} \neq F_x^{(C)}$, the difference between them being due to the integral over S_{ABMN} in Equations 15.27 and 15.31.

Equations 15.33 through 15.35 show that the problem for calculating F_x can be reduced to the calculation of the meniscus shape, $z = \zeta(x,y)$, and of the pressure tensor, $\mathbf{P}$, only in the midplane $x = 0$. This is a very important result because in the *middle* between the particles the meniscus slope is small, even if it is not small close to the particles. This fact allows us to considerably simplify the problem because of the following two reasons. First, for small meniscus slope the square root in Equation 15.34 can be expanded in series:

$$F_x^{(C)} = \frac{\gamma}{2} \int_{-\infty}^{\infty} \mathrm{d}y\, (\zeta_x^2 - \zeta_y^2)\big|_{x=0}. \qquad (15.38)$$

Second, in the region of small slope the Laplace equation of capillarity can be linearized. Hence, in this region the meniscus shape can be expressed as a superposition of the menisci created by the two particles in isolation:

$$\zeta(x,y) = \zeta_A(x,y) + \zeta_B(x,y) \qquad \text{(in the midplane } x = 0), \quad (15.39)$$

where ζ_A is the meniscus created by the left-hand-side particle if the other particle were missing, and ζ_B is the meniscus created by the right-hand-side particle if the other particle were missing. Equation 15.39 expresses a *superposition approximation*, which is applicable in all cases when the meniscus slope is small in the *middle* between the particles. (It is not necessary the slope to be small near the particles!) This approximation considerably simplifies the problem. It is worthwhile noting that a similar approximation was used by Verwey and Overbeek[132] to derive their very successful expression for the electrostatic disjoining pressure. For capillary forces, this approach was first applied in Ref. 106.

15.3.2 Application to Floating Noncharged Particles

The general expressions in Section 15.3.1 can be applied to the cases where gravitational and/or electric fields are present. Here, we consider the special case where only gravitational field is present, that is, two noncharged particles floating on a horizontal liquid interface. In such a case, the pressure tensor is isotropic in the two neighboring phases, "a" and "b":

$$\mathbf{P}_{\mathrm{a}} = (p_\infty - \rho_{\mathrm{a}} g z)\mathbf{U} \quad \text{and} \quad \mathbf{P}_{\mathrm{b}} = (p_\infty - \rho_{\mathrm{b}} g z)\mathbf{U}\,, \tag{15.40}$$

where p_∞ is the pressure at $z = 0$; $\mathbf{U}$ is the spatial unit tensor; ρ_{a} and ρ_{b} are the mass densities of the respective phases. Substituting Equation 15.40 into Equation 15.36, we obtain:

$$\begin{aligned} F_x^{(S)} &= \int_{-\infty}^{\infty} \mathrm{d}y \int_0^{\zeta} \mathrm{d}z\,(p_\infty - \rho_{\mathrm{a}} g z) - \int_{-\infty}^{\infty} \mathrm{d}y \int_0^{\zeta} \mathrm{d}z\,(p_\infty - \rho_{\mathrm{b}} g z) \\ &= -\int_{-\infty}^{\infty} \mathrm{d}y \int_0^{\zeta} \mathrm{d}z (\rho_{\mathrm{a}} - \rho_{\mathrm{b}}) g z = -\frac{1}{2}\gamma q^2 \int_{-\infty}^{\infty} \mathrm{d}y\, \zeta^2 \end{aligned}\,. \tag{15.41}$$

As before, q is the inverse capillary length:

$$q^2 \equiv \frac{(\rho_{\mathrm{a}} - \rho_{\mathrm{b}})g}{\gamma}\,. \tag{15.42}$$

Then, from Equations 15.33, 15.38 and 15.41, we obtain:[106]

$$F_x = -\frac{\gamma}{2} \int_{-\infty}^{\infty} \mathrm{d}y \left[q^2 \zeta^2 + \left(\frac{\partial \zeta}{\partial y}\right)^2 - \left(\frac{\partial \zeta}{\partial x}\right)^2 \right]\Big|_{x=0}\,. \tag{15.43}$$

Because we are using the assumption for small meniscus slope in the midplane, $x = 0$, we can substitute the superposition approximation, Equation 15.39, into Equation 15.43:

$$F_x = -\gamma \int_{-\infty}^{\infty} \mathrm{d}y \left(q^2 \zeta_A \zeta_B + \frac{\partial \zeta_A}{\partial y}\frac{\partial \zeta_B}{\partial y} - \frac{\partial \zeta_A}{\partial x}\frac{\partial \zeta_B}{\partial x}\right)\Bigg|_{x=0}, \qquad (15.44)$$

where we have used the fact that

$$F_x^{(Y)} = -\frac{\gamma}{2} \int_{-\infty}^{\infty} \mathrm{d}y \left[q^2 \zeta_Y^2 + \left(\frac{\partial \zeta_Y}{\partial y}\right)^2 - \left(\frac{\partial \zeta_Y}{\partial x}\right)^2\right]\Big|_{x=0} = 0, \quad Y = A, B, \qquad (15.45)$$

$F_x^{(A)}$ and $F_x^{(B)}$, given by Equation 15.45, are the forces acting on the *isolated* particles A and B, each of them being equal to zero. In view of Equation 15.1, in Equation 15.44 we substitute:

$$\zeta_A = Q_A K_0(q\rho_A), \qquad \zeta_B = Q_B K_0(q\rho_B), \qquad (15.46)$$

where ρ_A and ρ_B are the distances from a given point in the xy-plane to the centers of particles A and B (see Figure 15.8).

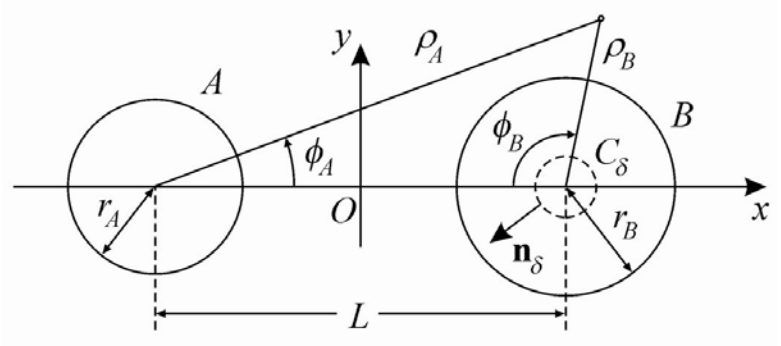

FIGURE 15.8 Polar coordinates (ρ_A,ϕ_A) and (ρ_B,ϕ_B) in the xy-plane connected with two particles, A and B. The projections of the contact lines on the particle surfaces are presented by two solid circles of radii r_A and r_B. The dashed circle C_δ, with outer unit normal $\mathbf{n}_\delta$, is an auxiliary contour used for the derivation of the expression for the capillary force.

Numerical solution of the integral in Equation 15.44, along with Equation 15.46 was carried out in Ref. 106 for two equal-sized particles, and it was found that the *numerical* result exactly coincides with the prediction of Equation 15.5, that is, the x-projection of force acting on the right-hand side particle is:

$$F_x = -2\pi\gamma Q_A Q_B q K_1(qL). \qquad (15.47)$$

To prove *analytically* that Equation 15.47 is an exact corollary of Equations 15.44 and 15.46 we have to first introduce the tensor of capillary interaction.

15.3.3 Obtaining the Force by Integrating the Tensor of Capillary Interaction

In the case of small meniscus slope, ζ_A and ζ_B obey the linearized Laplace equations of capillarity:

$$\frac{\partial^2 \zeta_A}{\partial x^2} + \frac{\partial^2 \zeta_A}{\partial y^2} = q^2 \zeta_A , \qquad \frac{\partial^2 \zeta_B}{\partial x^2} + \frac{\partial^2 \zeta_B}{\partial y^2} = q^2 \zeta_B . \tag{15.48}$$

Introducing the notations

$$x_1 \equiv x \quad \text{and} \quad x_2 \equiv y , \tag{15.49}$$

we define the symmetric two-dimensional tensor T_{kn} as follows:

$$T_{kn} \equiv \frac{\partial \zeta_A}{\partial x_k}\frac{\partial \zeta_B}{\partial x_n} + \frac{\partial \zeta_A}{\partial x_n}\frac{\partial \zeta_B}{\partial x_k} - (\frac{\partial \zeta_A}{\partial x_j}\frac{\partial \zeta_B}{\partial x_j} + q^2 \zeta_A \zeta_B)\delta_{kn} , \tag{15.50}$$

(k,n = 1,2) where δ_{kn} is the 2D Kronecker symbol and summation is assumed over the repeated index j (the Einstein rule). By using Equations 15.48 through 15.50, we can prove that[93]

$$\frac{\partial T_{kn}}{\partial x_k} = 0 , \qquad n = 1,2 , \tag{15.51}$$

that is, $\nabla \cdot \mathbf{T} = 0$, in tensorial notations. Integrating the latter relation over a domain S_+, which represents the right half of the xy-plane, corresponding to $x > 0$, except a circle, C_δ, around the center of particle B (Figure 15.8), we obtain:

$$\mathbf{0} = -\int_{S_+} dS \, \nabla \cdot \mathbf{T} = \int_{-\infty}^{\infty} \mathrm{d}y \, \mathbf{e}_x \cdot \mathbf{T}\big|_{x=0} + \int_{C_\delta} \mathrm{d}l \, \mathbf{n}_\delta \cdot \mathbf{T} , \tag{15.52}$$

where $\mathbf{n}_\delta$ is the outer unit normal field of the contour C_δ. Taking the x-projection of the latter equation, in view of Equation 15.50, we derive:

$$\int_{-\infty}^{\infty} \mathrm{d}y \, (q^2 \zeta_A \zeta_B + \frac{\partial \zeta_A}{\partial y}\frac{\partial \zeta_B}{\partial y} - \frac{\partial \zeta_A}{\partial x}\frac{\partial \zeta_B}{\partial x})\big|_{x=0} = \int_{C_\delta} \mathrm{d}l \, \mathbf{n}_\delta \cdot \mathbf{T} \cdot \mathbf{e}_x . \tag{15.53}$$

Finally, the combination of Equations 15.44 and 15.53 yields:

$$F_x = -\gamma \int_{C_\delta} \mathrm{d}l \, \mathbf{n}_\delta \cdot \mathbf{T} \cdot \mathbf{e}_x . \tag{15.54}$$

In the following, Equation 15.54 is used for calculating the force of capillary interaction for various capillary multipoles, including capillary charges (m = 0). Because the tensor $\mathbf{T}$, defined by Equation 15.50 is used for this purpose, it has been called *the tensor of capillary interaction*.[93] The way in which Equation 15.54 is applied to derive Equation 15.47 is demonstrated in the next section.

15.4 INTERACTIONS BETWEEN CAPILLARY MULTIPOLES

15.4.1 Integral Expression for the Capillary Force

Here, following Ref. 93, we apply Equation 15.54 for deriving expressions for the lateral capillary force between various capillary multipoles. As before, the left- and right-hand side particles are denoted as "particle *A*" and "particle *B*", respectively (Figure 15.8). In the general case, the meniscus around each particle in isolation can be expressed as a Fourier expansion[56]

$$\zeta_Y(x,y) = \sum_{m=0}^{\infty} h_{Y,m} \frac{K_m(q\rho_Y)}{K_m(qr_Y)} \cos[m(\phi_Y - \phi_{Y,m})], \quad Y = A, B, \tag{15.55}$$

where small meniscus slope is presumed; K_m is the modified Bessel functions of second kind and order m (m = 0, 1, …); $h_{Y,m}$ and $\phi_{Y,m}$ are the amplitude and phase shift for the mth mode of undulation of the particle contact line; r_Y ($Y = A$, B) is the radius of its vertical projection on the xy-plane (Figure 15.8). The capillary charge of the particle (corresponding to m = 0) is:

$$Q_Y \equiv -\frac{h_{Y,0}}{K_0(qr_Y)}, \qquad Y = A, B, \tag{15.56}$$

where (ρ_A,ϕ_A) and (ρ_B,ϕ_B) are polar coordinates associated, respectively, with the left- and right-hand side particle (Figure 15.8):

$$x \equiv -\frac{L}{2} + \rho_A \cos\phi_A \quad \text{and} \quad y \equiv \rho_A \sin\phi_A, \tag{15.57}$$

$$x \equiv \frac{L}{2} - \rho_B \cos\phi_B \quad \text{and} \quad y \equiv \rho_B \sin\phi_B. \tag{15.58}$$

For the right-hand side particle, Equation 15.54 acquires the form:

$$F_x = -\gamma r_\delta \int_0^{2\pi} \mathrm{d}\phi_B \, \mathbf{e}_\rho \cdot \mathbf{T} \cdot \mathbf{e}_x \quad \text{at} \quad \rho_B = r_\delta, \tag{15.59}$$

where $\mathbf{e}_\rho$ is a radial unit vector; r_δ is the radius of the contour C_δ. The way of derivation of Equation 15.54 implies that F_x must be the same independently of the choice of r_δ (see above). In what follows, we will use the transition $r_\delta \to 0$; see Equations 15.65 through 15.68 below. This transition is possible because the Fourier expansion, Equation 15.55, defines the

functions $\zeta_A(\rho_A,\phi_A)$ and $\zeta_B(\rho_B,\phi_B)$ in the whole *xy*-plane. The poles of ζ_A in the point $\rho_A = 0$, and of ζ_B in the point $\rho_B = 0$, do not represent an obstacle for the derivation of expressions for the physical quantities. In fact, the method based on the limiting transition $r_\delta \to 0$ is equivalent to the method of residues applied in Ref. 56.

With the help of Equations 15.50 and 15.58, we can represent Equation 15.59 in the form:[93]

$$F_x = \gamma r_\delta \int_0^{2\pi} [\frac{\partial \zeta_A}{\partial \rho_B}\frac{\partial \zeta_B}{\partial \rho_B}\cos\phi_B - (\frac{\partial \zeta_A}{\partial \phi_B}\frac{\partial \zeta_B}{\partial \rho_B} + \frac{\partial \zeta_A}{\partial \rho_B}\frac{\partial \zeta_B}{\partial \phi_B})\frac{\sin\phi_B}{r_\delta}$$

$$-(\frac{1}{{r_\delta}^2}\frac{\partial \zeta_A}{\partial \phi_B}\frac{\partial \zeta_B}{\partial \phi_B} + q^2\zeta_A\zeta_B)\cos\phi_B]\,\mathrm{d}\phi_B \quad \text{at} \quad \rho_B = r_\delta . \tag{15.60}$$

The latter equation will be applied for calculating the force of interaction between various capillary multipoles (see below).

15.4.2 Interaction of a Capillary Charge with Capillary Multipoles

Let us consider the case, in which the particle *B* is a capillary charge. Then, only the term with $m = 0$ remains in the Fourier expansion for ζ_B; see Equation 15.55. Then, $\zeta_B = \zeta_B(\rho_B)$; all terms containing the derivative $\partial\zeta_B/\partial\phi_B$ disappear, and Equation 15.60 reduces to:

$$F_x = \gamma r_\delta \int_0^{2\pi} [(\frac{\partial \zeta_A}{\partial \rho_B}\cos\phi_B - \frac{\partial \zeta_A}{\partial \phi_B}\frac{\sin\phi_B}{\rho_B})\frac{\partial \zeta_B}{\partial \rho_B} - q^2\zeta_A\zeta_B\cos\phi_B]\,\mathrm{d}\phi_B \quad \text{at} \quad \rho_B = r_\delta . \tag{15.61}$$

With the help of Equation 15.58, we can check that

$$\frac{\partial \zeta_A}{\partial \rho_B}\cos\phi_B - \frac{\partial \zeta_A}{\partial \phi_B}\frac{\sin\phi_B}{\rho_B} = -\frac{\partial \zeta_A}{\partial x} . \tag{15.62}$$

Next, in Equation 15.61 we apply the limiting transition $r_\delta \to 0$; see the discussion after Equation 15.59. Having in mind that $\zeta_B \propto K_0(q\rho_B)$, we obtain:

$$F_x = -2\pi\gamma[\frac{\partial \zeta_A}{\partial x}(r_\delta \frac{\partial \zeta_B}{\partial \rho_B})]\Big|_{\rho_B = r_\delta \to 0} . \tag{15.63}$$

From Equation 15.55, along with Equation 15.56 we derive:

$$(r_\delta \frac{\partial \zeta_B}{\partial \rho_B})\Big|_{\rho_B = r_\delta \to 0} = -Q_B[r_\delta \frac{\partial K_0(q\rho_B)}{\partial \rho_B}]\Big|_{\rho_B = r_\delta \to 0} = Q_B . \qquad (15.64)$$

Substituting Equation 15.64 into Equation 15.63, we obtain:

$$F_x = -2\pi\gamma Q_B (\frac{\partial \zeta_A}{\partial x})\Big|_{r_\delta \to 0} . \qquad (15.65)$$

Equation 15.57 yields:

$$\rho_A^2 = (\frac{L}{2} + x)^2 + y^2 \quad \text{and} \quad \tan\phi_A = \frac{2y}{L+2x} \quad . \qquad (15.66)$$

In addition, for $r_\delta \to 0$ we have $x \to L/2$ and $y \to 0$. Hence,

$$\frac{\partial \rho_A}{\partial x}\Big|_{r_\delta \to 0} = 1 \quad \text{and} \quad \frac{\partial \phi_A}{\partial x}\Big|_{r_\delta \to 0} = 0 . \qquad (15.67)$$

First, let us assume that the particle A is a *capillary charge*, i.e. $\zeta_A = -Q_A K_0(q\rho_A)$. Then, with the help of Equation 15.67 we derive:

$$(\frac{\partial \zeta_A}{\partial x})\Big|_{r_\delta \to 0} = \frac{\partial}{\partial x}[-Q_A K_0(q\rho_A)]\Big|_{r_\delta \to 0} = q Q_A K_1(qL) . \qquad (15.68)$$

The combination of Equations 15.65 and 15.68 gives exactly the known expression for the capillary force, Equation 15.47. An equivalent form of Equation 15.47 can be obtained if we use Equation 15.56, along with the identity $K_1(qL) = K_{-1}(qL)$:[93]

$$F_x = -\pi\gamma q h_{A,0} h_{B,0} \frac{K_1(qL) + K_{-1}(qL)}{K_0(qr_A)K_0(qr_B)} \quad \text{(charge-charge)}. \qquad (15.69)$$

The latter presentation of the force between two capillary charges ($m = 0$) is useful, because it allows generalization for capillary multipoles of arbitrary order; see Equations 15.71 and 15.78 below. The advantage of the present method, which based on the transition $r_\delta \to 0$, is that it allows us to derive (relatively simply) such generalized expressions.

Second, let us assume that the particle A is a *capillary multipole* of order m, while the particle B is a capillary charge ($m = 0$), as before. In such a case, in view of Equations 15.55, 15.65 and 15.67, we obtain:

$$\left(\frac{\partial \zeta_A}{\partial x}\right)\Bigg|_{r_\delta \to 0} = -\frac{\partial}{\partial x}\{h_{A,m}\frac{K_m(q\rho_A)}{K_m(qr_A)}\cos[m(\phi_A - \phi_{A,m})]\}\Bigg|_{\rho_B = r_\delta \to 0}$$

$$= -\frac{qh_{A,m}}{2}\frac{K_{m+1}(qL) + K_{m-1}(qL)}{K_m(qr_A)}\cos(m\phi_{A,m}). \qquad (15.70)$$

Substituting Equation 15.70 into Equation 15.65 we derive the expression for the charge-multipole capillary interaction force:

$$F_x = -\pi\gamma\, qh_{A,m}h_{B,0}\frac{K_{m+1}(qL) + K_{m-1}(qL)}{K_m(qr_A)K_0(qr_B)}\cos(m\phi_{A,m}) \quad \text{(charge-multipole)} \quad (15.71)$$

(m = 0, 1, 2, …), where Equation 15.56 has been used for $Y = B$. Substituting $m = 0$ in Equation 15.71, we obtain Equation 15.69. Integrating Equation 15.71 with respect to L, we obtain an expression for the interaction energy:

$$\Delta W = 2\pi\gamma\, h_{A,m}Q_B\frac{K_m(qL)}{K_m(qr_A)}\cos(m\phi_{A,m}) \quad \text{(charge-multipole)} \qquad (15.72)$$

(m = 0, 1, 2, …), where Equation 15.56 has been used again for $Y = B$.

In the case of $qL << 1$, Equation 15.71 reduces to:

$$F_x \approx 2m\pi\gamma\, h_{A,m}Q_B\frac{r_A^m}{L^{m+1}}\cos(m\phi_{A,m}) \quad \text{(charge-multipole for } qL << 1), \qquad (15.73)$$

which is valid for $m \geq 1$. Integrating Equation 15.73 we obtain the respective asymptotic expression for the energy of capillary interaction:

$$\Delta W \approx 2\pi\gamma\, h_{A,m}Q_B\frac{r_A^m}{L^m}\cos(m\phi_{A,m}) \quad \text{(charge-multipole for } qL << 1) \qquad (15.74)$$

(m = 1, 2, …). Equation 15.74 is the correct asymptotic expression for ΔW. In Ref. 56, see Table 2 therein, the factor 2π in the right-hand side of Equation 15.74 is given (by mistake) as $\pi/2$.

15.4.3 Interactions between Capillary Multipoles of Arbitrary Order

Here, we consider the general case where the particle A is a capillary multipole of order m, whereas the particle B is a capillary multipole of order n (m, n = 1, 2, …); see also Figure 15.8. Because we are using the limiting transition $\rho_B = r_\delta \to 0$, we can work, from the very beginning, with the expression for ζ_B in its form for small ρ_B:

$$\zeta_B(x,y) \approx \frac{h_{B,n}}{K_n(qr_B)} \frac{2^{n-1}(n-1)!}{(q\rho_B)^n} \cos[n(\phi_B - \phi_{B,n})] \quad \text{for } n \geq 1, \tag{15.75}$$

see Equation 15.55. Substituting Equation 15.75 into Equation 15.60, after some mathematical transformations we obtain:[93]

$$F_x = -\frac{2^{n-1}\gamma h_{B,n}}{q^n K_n(qr_B)} \int_0^{2\pi} \frac{n!}{r_\delta{}^n} \left[\frac{\partial \zeta_A}{\partial \rho_B} + \frac{n+1}{r_\delta}\zeta_A\right]\Big|_{\rho_B = r_\delta} \cos[(n+1)\phi_B - n\phi_{B,n}]\,\mathrm{d}\phi_B \,. \tag{15.76}$$

Next, in Equation 15.76 we substitute the expression for ζ_A for a capillary multipole of order m, and after some transformations we derive:[93]

$$F_x = -\frac{2^n \gamma h_{A,m} h_{B,n}}{q^n K_m(qr_A) K_n(qr_B)} \int_0^{2\pi} \frac{\partial^{n+1}}{\partial \rho_B^{n+1}} \left\{K_m(q\rho_A)\cos[m(\phi_A - \phi_{A,m})]\right\}\Big|_{\rho_B = r_\delta \to 0}$$

$$\times \cos[(n+1)\phi_B - n\phi_{B,n}]\,\mathrm{d}\phi_B \,. \tag{15.77}$$

From Equation 15.77, after long and nontrivial calculations, the general expression for the force of interaction between two capillary multipoles of orders m and n was derived in Ref. 93:

$$F_x = -\frac{\pi\gamma q h_{A,m} h_{B,n}}{2K_m(qr_A)K_n(qr_B)} [K_{m+n+1}(qL)\cos(m\phi_{A,m} - n\phi_{B,n}) + K_{m-n-1}(qL)\cos(m\phi_{A,m} + n\phi_{B,n})] \tag{15.78}$$

(m, n = 1, 2, 3, …). In the asymptotic case of small particles, qL <<1, Equation 15.78 reduces to:

$$F_x \approx -2\pi \frac{(m+n)!}{(m-1)!(n-1)!} \gamma h_{A,m} h_{B,n} \frac{r_A^m r_B^n}{L^{m+n+1}} \cos(m\phi_{A,m} - n\phi_{B,n}) \quad \text{for } qL << 1. \tag{15.79}$$

Integrating Equation 15.79, we obtain the energy of capillary interaction between *m*- and *n*-multipoles:

$$\Delta W \approx -2\pi \frac{(m+n-1)!}{(m-1)!(n-1)!} \gamma h_{A,m} h_{B,n} \frac{r_A^m r_B^n}{L^{m+n}} \cos(m\phi_{A,m} - n\phi_{B,n}) \quad \text{for } qL << 1. \qquad (15.80)$$

One can check that Equation 15.80 is identical to the respective expression in Ref. 56, having in mind that the phase-shift angles in Ref. 56 are defined as $\pi - \phi_{Y,m}$, where $\phi_{Y,m}$ is the phase-shift angle in the present chapter ($Y = A, B$; $m = 1, 2, \ldots$).

Equation 15.78 is more general than Equation 15.79, the latter representing a special case at $qL << 1$. The capillary interaction energy, ΔW, obtained by integration of the general Equation 15.78, is:

$$\Delta W = -\frac{\pi\gamma h_{A,m} h_{B,n}}{2K_m(qr_A)K_n(qr_B)} [G_{m+n+1}(qL)\cos(m\phi_{A,m} - n\phi_{B,n}) + G_{m-n-1}(qL)\cos(m\phi_{A,m} + n\phi_{B,n})] \quad , \qquad (15.81)$$

where $m, n = 1, 2, \ldots$, and

$$G_j(qL) \equiv \int_{qL}^{\infty} K_j(\xi)\,\mathrm{d}\xi, \qquad j = \pm 1, \pm 2, \ldots. \qquad (15.82)$$

The integral in Equation 15.82 cannot be solved analytically, and numerical integration should be applied. For this reason, it is simpler to calculate the force from Equation 15.78 than the energy from Equation 15.81.

In summary, in this section we considered the interaction between capillary multipoles of various orders, $m, n = 0, 1, 2, 3, \ldots$, under the assumption that the meniscus slope is small, i.e. $\zeta_x^2 + \zeta_y^2 << 1$. As a rule, this assumption is fulfilled for millimeter-sized and smaller particles. The derived analytical expressions for the interaction between capillary charge and multipole, Equations 15.71 and 15.72, and between two capillary multipoles, Equations 15.78 and 15.81, are more general that the previously published ones,[56] which have been derived using the additional assumption $qL << 1$. Note also that in Ref. 56 we used the *energy approach*, that is, ΔW was calculated, and then the force F_x was obtained by differentiation. In contrast, in this section we used the *force approach*, which in based on the calculation of F_x, and then the interaction energy, ΔW, is obtained by integration. Of course, if correctly applied, the two approaches yield identical results.

15.5 ELECTROCAPILLARY INTERACTION

15.5.1 Meniscus Profile in the Presence of Electric Field

Here, following Ref. 103, we consider two electrically charged particles, like those in Figure 15.1c, which are located at the boundary between water and a nonpolar fluid (oil or air). In other words, phase "a" is the water and phase "b" is the nonpolar fluid. The charged particles create electric field, which in its own turn gives rise to mechanical stresses described by the Maxwell pressure tensor:

$$\mathbf{P}_{\mathrm{w}} = (p_{\mathrm{w}} + \frac{\varepsilon_{\mathrm{w}}}{8\pi}\nabla\varphi_{\mathrm{w}} \cdot \nabla\varphi_{\mathrm{w}})\mathbf{U} - \frac{\varepsilon_{\mathrm{w}}}{4\pi}\nabla\varphi_{\mathrm{w}}\nabla\varphi_{\mathrm{w}}, \tag{15.83}$$

$$\mathbf{P}_{\mathrm{n}} = (p_{\mathrm{n}} + \frac{\varepsilon_{\mathrm{n}}}{8\pi}\nabla\varphi_{\mathrm{n}} \cdot \nabla\varphi_{\mathrm{n}})\mathbf{U} - \frac{\varepsilon_{\mathrm{n}}}{4\pi}\nabla\varphi_{\mathrm{n}}\nabla\varphi_{\mathrm{n}}, \tag{15.84}$$

where the subscripts "w" and "n" denote quantities related, respectively, to the water and nonpolar-fluid phases. In particular, p_{w} and p_{n} are the scalar (hydrostatic) pressures in the respective phases, whereas φ_{w} and φ_{n} are the fields of the electrostatic potential therein. The substitution of Equations 15.83 and 15.84 into the right-hand side of the Laplace equation of capillarity, Equation 15.22, yields:

$$2H\gamma_{\mathrm{a}} = p_{\mathrm{n}} + \frac{\varepsilon_{\mathrm{n}}}{8\pi}[(\mathbf{n}_{\mathrm{s}} \times \nabla\varphi_{\mathrm{n}})^2 - (\mathbf{n}_{\mathrm{s}} \cdot \nabla\varphi_{\mathrm{n}})^2]$$

$$- p_{\mathrm{w}} - \frac{\varepsilon_{\mathrm{w}}}{8\pi}[(\mathbf{n}_{\mathrm{s}} \times \nabla\varphi_{\mathrm{w}})^2 - (\mathbf{n}_{\mathrm{s}} \cdot \nabla\varphi_{\mathrm{w}})^2] \quad \text{at} \quad z = \zeta, \tag{15.85}$$

where we have used the vectorial identity $\mathbf{A}^2\mathbf{B}^2 = (\mathbf{A}\times\mathbf{B})^2 + (\mathbf{A}\cdot\mathbf{B})^2$ with $\mathbf{A} = \mathbf{n}_{\mathrm{s}}$ and $\mathbf{B} = \nabla\varphi$.

In what follows, we will restrict our considerations to the case, where the electric charges are located at the particle/nonpolar-fluid interface. This case has been observed experimentally with various systems.[58–70] The dielectric constant of water, ε_{w}, is usually much greater than those of the particle, ε_{p}, and of the nonpolar fluid, ε_{n}: i.e. $\varepsilon_{\mathrm{w}} >> \varepsilon_{\mathrm{p}}, \varepsilon_{\mathrm{n}}$. For this reason, the electric field created by charges, located at the particle/nonpolar-fluid interface, practically does not penetrate into the water phase; see, for example, the known problems for the image-charge effect[96,97] and for a hydrophobic particle near an oil-water interface.[98] Experimentally, the non-penetration of the field into water is manifested as independence of the configuration of the adsorbed particles on the electrolyte concentration in the aqueous phase.[58,60,64] Thus, in first approximation, the role of the water is to keep the electric potential constant at the particle/water and water/nonpolar-fluid interfaces. In such a case, we can set $\varphi_{\mathrm{w}} \equiv 0$, and

$$\varphi_{\rm n} = 0 \quad \text{at} \quad z = \zeta(x,y)\,. \tag{15.86}$$

In other words, the interface $z = \zeta(x,y)$ is equipotential, and then the vector $\nabla\varphi_{\rm n}$ is directed along the normal $\mathbf{n}_{\rm s}$. Setting $\varphi_{\rm w} = 0$ and $\mathbf{n}_{\rm s}\times\nabla\varphi_{\rm n} = 0$ in Equation 15.85, and using the assumption for small meniscus slope, we obtain:

$$\frac{\partial^2\zeta}{\partial x^2} + \frac{\partial^2\zeta}{\partial y^2} = -\frac{\varepsilon_{\rm n}}{8\pi\gamma}\left(\frac{\partial\varphi_{\rm n}}{\partial z}\right)^2 \quad \text{at} \quad z = \zeta\,. \tag{15.87}$$

We have used also the fact that if the liquid interface is flat far from the particles, then $p_{\rm n} = p_{\rm w}$. (In the present section we will neglect the effect of the gravitational hydrostatic pressure, which is negligible for small particles.) Equation 15.87, along with the boundary condition, Equation 15.86, allows us to calculate the deformation of the liquid interface created by the particles and their electric field, as well as the force of interaction between the particles. For this goal, we will apply the following *iteration procedure*:

1. The electrostatic potential in zero-order approximation, $\varphi_0(\mathbf{r})$, will be calculated assuming that the liquid interface is flat and equipotential, that is, $\varphi_0|_{z=0} = 0$.

2. Next, substituting $\varphi_{\rm n} = \varphi_0$ in the right-hand side of Equation 15.87, we will find the meniscus shape, $z = \zeta(x,y)$, in first approximation. After that, we will determine the surface tension contribution to the interaction force, $F_x^{(\gamma)}$; see Section 15.5.2.

3. To find the next correction term, we will seek $\varphi_{\rm n}$ in the form:

$$\varphi_{\rm n} = \varphi_0(\mathbf{r}) + \varphi_1(\mathbf{r})\,, \tag{15.88}$$

where φ_1 accounts for the fact that the deformation of the liquid interface affects the field of the electrostatic potential $\varphi_{\rm n}$. Expanding in series the boundary condition, Equation 15.86, we obtain $0 = \varphi_{\rm n}(x,y,\zeta(x,y)) = \varphi_{\rm n}(x,y,0) + (\partial\varphi_{\rm n}/\partial z)_{z=0}\zeta + \ldots$. Substituting Equation 15.88 we get:

$$\varphi_1 = -\frac{\partial\varphi_0}{\partial z}\zeta \quad \text{at} \quad z = 0\,. \tag{15.89}$$

Thus, φ_1 is solution of the equation $\nabla^2\varphi_1 = 0$ (no ions in the nonpolar fluid), along the boundary condition 15.89.

4. With $\varphi_{\rm n} = \varphi_0(\mathbf{r}) + \varphi_1(\mathbf{r})$, we calculate the Maxwell pressure tensor, $\mathbf{P}$, and then by using Equation 15.24 we determine $F_x^{(\rm p)}$. Thus, we find the total interaction force, $F_x = F_x^{(\gamma)} + F_x^{(\rm p)}$.

The next step in the iteration procedure would be to substitute $\varphi_n = \varphi_0(\mathbf{r}) + \varphi_1(\mathbf{r})$ in the right-hand side of Equation 15.87 and to determine the next correction in the meniscus profile $\zeta(x,y)$. However, it turns out that the resulting correction term is of the order of the neglected term in Equation 15.87, $\zeta_x^2 + \zeta_y^2 << 1$, and hence this correction term is negligible in the framework of the assumption for small meniscus slope. For this reason, we stop the iterations after completing step 4.

15.5.2 Calculation of $F_x^{(\eta)}$ for Two Particles with Dipolar Fields

As mentioned above, an adsorbed charged particle creates an electric field, which has asymptotically dipolar character because of the image-charge effect (see Figure 15.5). For this reason, in zero-order approximation we will assume that the electric field created by the two particles, A and B, in the nonpolar fluid is equivalent to the superposition of the fields of two dipoles:

$$\varphi_0 = \varphi_{A,0} + \varphi_{B,0}, \tag{15.90}$$

$$\varphi_{A,0} = \frac{p_d}{\varepsilon_n} \frac{z}{(\rho_A^2 + z^2)^{3/2}} \quad \text{and} \quad \varphi_{B,0} = \frac{p_d}{\varepsilon_n} \frac{z}{(\rho_B^2 + z^2)^{3/2}}, \tag{15.91}$$

where p_d is the dipole moment; as before, ρ_A and ρ_B are position vectors with respect to the particle centers (Figure 15.8); A and B are two identical particles separated at a center-to-center distance L (Figure 15.9).

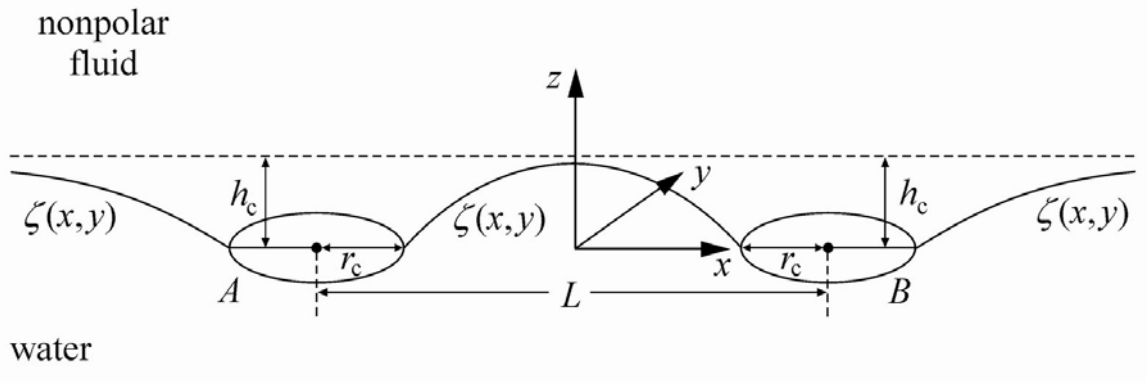

FIGURE 15.9 Sketch of the meniscus profile, $z = \zeta(x,y)$, around two identical charged particles, A and B, which are attached to the boundary between a water phase and a nonpolar fluid (e.g., air or oil). The contact lines on the particle surfaces are presented by two solid circles of radius r_c. The distance between the plane of the contact lines and the plane of the non-perturbed interface far from the particles is denoted by h_c.

First, to determine the profile, $z = \zeta_A(x,y)$ or $z = \zeta_B(x,y)$, of the meniscus around each of the two particles *in isolation*, in the right-hand side of Equation 15.87 we substitute $\varphi_n = \varphi_{Y,0}$, $Y = A, B$, from Equation 15.91, which leads to:

$$\frac{1}{\rho_Y}\frac{d}{d\rho_Y}\left(\rho_Y \frac{d\zeta_Y}{d\rho_Y}\right) = -\frac{p_d^2}{8\pi\gamma\varepsilon_n\rho_Y^6}, \quad Y = A, B. \tag{15.92}$$

The first integral of Equation 15.92 is:

$$\frac{d\zeta_Y}{d\rho_Y} = \frac{p_d^2}{32\pi\gamma\varepsilon_n\rho_Y^5}, \quad Y = A, B. \tag{15.93}$$

Setting $\rho_Y = r_c$ in Equation 15.93, we determine the meniscus slope at the contact line (Figure 15.9):

$$\delta \equiv \tan\psi_c = \frac{p_d^2}{32\pi\gamma\varepsilon_n r_c^5}. \tag{15.94}$$

Insofar as the meniscus slope is small, δ is a small parameter, which will be used below. Furthermore, having in mind that the electrodipping force, F_{ED}, acting on each particle is counterbalanced by the vertical component of the surface tension force, $F_{ED} = 2\pi\gamma r_c \sin\psi_c$ (Figure 15.3), from Equation 15.94 we obtain:

$$F_{ED} = \frac{p_d^2}{16\varepsilon_n r_c^4} \tag{15.95}$$

($\sin\psi_c \approx \tan\psi_c$ at small meniscus slope). The subsequent integration of Equation 15.93 yields the following expression for the meniscus shape around an isolated particle:

$$\zeta_Y = \frac{p_d^2}{128\pi\gamma\varepsilon_n}\left(\frac{1}{r_c^4} - \frac{1}{\rho_Y^4}\right), \quad Y = A, B. \tag{15.96}$$

As already mentioned, in the present section we neglect the gravitational effects (for small particles), so that $\zeta_Y(\rho_Y)$ is determined by the particle electric field. Here, we have assumed that the *xy*-plane coincides with the plane of the particles' contact line, which is located at a distance h_c below the plane of the non-disturbed liquid interface far from the particles (Figure 15.9). Setting $\rho_Y \to \infty$ in Equation 15.96, we find:

$$h_{\mathrm{c}} = \frac{p_{\mathrm{d}}^2}{128\pi\gamma\varepsilon_{\mathrm{n}} r_{\mathrm{c}}^4}. \tag{15.97}$$

Next, to determine the profile $z = \zeta(x,y)$ of the meniscus around the pair of two particles (Figure 15.9), in the right-hand side of Equation 15.87 we substitute $\varphi_{\mathrm{n}} = \varphi_{A,0} + \varphi_{B,0}$ from Equation 15.91, which leads to:

$$\frac{\partial^2\zeta}{\partial x^2} + \frac{\partial^2\zeta}{\partial y^2} = -\frac{p_{\mathrm{d}}^2}{8\pi\gamma\varepsilon_{\mathrm{n}}}\left(\frac{1}{\rho_A^6} + \frac{2}{\rho_A^3\rho_B^3} + \frac{1}{\rho_B^6}\right). \tag{15.98}$$

One can check that a particular solution to the inhomogeneous Equation 15.98 is:

$$\zeta_{\mathrm{inh}} \equiv -\frac{p_{\mathrm{d}}^2}{128\pi\gamma\varepsilon_{\mathrm{n}}}\left(\frac{1}{\rho_A^4} + \frac{1}{\rho_B^4}\right) + \frac{p_{\mathrm{d}}^2}{4\pi\gamma\varepsilon_{\mathrm{n}} L^2}\left(\frac{1}{\rho_A\rho_B} - 2\frac{\rho_A^2 + \rho_B^2}{\rho_A\rho_B L^2}\right), \tag{15.99}$$

where we have used the fact that (Figure 15.8)

$$\rho_A^2 = (x + L/2)^2 + y^2, \qquad \rho_B^2 = (x - L/2)^2 - y^2. \tag{15.100}$$

The solution of Equation 15.98 represents the sum of $\zeta_{\mathrm{inh}}(x,y)$ plus the solution of the respective homogeneous equation, $\zeta_{\mathrm{h}}(x,y)$, that is,

$$\zeta = \zeta_{\mathrm{inh}} + \zeta_{\mathrm{h}}, \quad \text{where} \quad \frac{\partial^2\zeta_{\mathrm{h}}}{\partial x^2} + \frac{\partial^2\zeta_{\mathrm{h}}}{\partial y^2} = 0. \tag{15.101}$$

Because $\zeta = 0$ at the particle's contact line (Figure 15.9), the respective boundary conditions for ζ_{h} read:

$$\zeta_{\mathrm{h}} = -\zeta_{\mathrm{inh}} \quad \text{at} \quad \rho_A = r_{\mathrm{c}} \quad \text{and} \quad \rho_B = r_{\mathrm{c}}, \tag{15.102}$$

where ζ_{inh} is given by Equation 15.99. Having determined $\zeta(x,y)$, we can calculate the x-projection of the interaction force $\mathbf{F}^{(\gamma)}$ acting on the right-hand side particle by using Equation 15.24:

$$\begin{aligned} F_x^{(\gamma)} &= -\gamma r_{\mathrm{c}} \int_0^{2\pi} [1 + (\frac{\partial\zeta}{\partial\rho_B})^2]^{-1/2} \cos\phi_B \, \mathrm{d}\phi_B \\ &\approx \frac{\gamma r_{\mathrm{c}}}{2} \int_0^{2\pi} (\frac{\partial\zeta}{\partial\rho_B})^2 \cos\phi_B \, \mathrm{d}\phi_B \quad \text{at} \quad \rho_B = r_{\mathrm{c}} \end{aligned}. \tag{15.103}$$

The function $\zeta_h(x,y)$ was found in Ref. 103 in the form of Fourier expansion by solving Equation 15.101 in bipolar coordinates. Next, $\zeta = \zeta_{inh} + \zeta_h$ was substituted in Equation 15.103 and the integration was carried out. The result was obtained in the form of a series expansion with respect to the powers of r_c/L:

$$F_x^{(\gamma)} = \frac{p_d^4}{2\pi\gamma\varepsilon_n^2 r_c^9} f_x^{(\gamma)}, \tag{15.104}$$

$$f_x^{(\gamma)} = \frac{3}{64}\left(\frac{r_c}{L}\right)^4 - \frac{1}{256}\left(\frac{r_c}{L}\right)^5 - \frac{93}{512}\left(\frac{r_c}{L}\right)^6 + \frac{91}{256}\left(\frac{r_c}{L}\right)^7 + \frac{1}{4096}\left(\frac{r_c}{L}\right)^8 - \frac{421}{256}\left(\frac{r_c}{L}\right)^9 + O\left(\frac{r_c^{10}}{L^{10}}\right). \tag{15.105}$$

The positive sign of the first term in the right-hand side of Equation 15.105 means that at long interparticle distances, $F_x^{(\gamma)}$ corresponds to *repulsion*. To see what is the total interaction force, we also have to calculate also $F_x^{(p)}$.

15.5.3 Calculation of $F_x^{(p)}$ and of the Total Electrocapillary Force

The force experienced by a dipole of moment **p** is $\mathbf{F} = \mathbf{p}\cdot\nabla\mathbf{E}$, where **E** is the intensity of the applied external electric field (the field of the considered dipole **p** being excluded).[133] With $\mathbf{p} = p_d\mathbf{e}_z$ and $\mathbf{E} = -\nabla(\varphi_{A,0} + \varphi_1)$, we find the x-projection of the force $F^{(p)}$ acting on the particle B:

$$F_x^{(p)} = -\frac{p_d}{2}\frac{\partial}{\partial z}\left(\frac{\partial\varphi_{A,0}}{\partial x} + \frac{\partial\varphi_1}{\partial x}\right) = \frac{3p_d^2}{2\varepsilon_n L^4} - \frac{p_d}{2}\frac{\partial^2\varphi_1}{\partial x\partial z} \text{ at } x = \frac{L}{2},\ y = z = 0, \tag{15.106}$$

where we have substituted $\varphi_{A,0}$ from Equation 15.91. In Equation 15.106, the factor 1/2 appears because the electric field is present only in the upper half-space (Figure 15.5). Thus, to calculate $F_x^{(p)}$ we have to first determine φ_1. We recall that φ_1 satisfies the Laplace Equation $\nabla^2\varphi_1 = 0$, along with the boundary condition (Equation 15.89). At given boundary condition for φ_1 in the plane $z = 0$, we can calculate φ_1 in the upper half-space ($z > 0$) by using the known Green function for the Dirichlet boundary problem:

$$\varphi_1(x,y,z) = \frac{1}{2\pi}\int_{-\infty}^{\infty}\int_{-\infty}^{\infty}\frac{z\varphi_s(\tilde{x},\tilde{y})}{[(x-\tilde{x})^2+(y-\tilde{y})^2+z^2]^{3/2}}\,\mathrm{d}\tilde{x}\,\mathrm{d}\tilde{y}\,, \qquad (15.107)$$

where $\tilde{x}$ and $\tilde{y}$ are integration variables. In view of Equation 15.89, the function φ_s is defined as follows:

$$\varphi_s = -\zeta\left.\frac{\partial\varphi_0}{\partial z}\right|_{z=0}\,, \qquad (15.108)$$

where the definition of ζ is extended as $\zeta \equiv 0$ in the circles $\rho_A < r_c$ and $\rho_B < r_c$; see Figure 15.9. In Equations 15.107 and 15.108, φ_0 can be substituted from Equations 15.90 and 15.91, and $\zeta(x,y)$ – from the series expansion derived in Ref. 103. As a result, from Equations 15.106 through 15.108 we arrive at an expression for $F_x^{(p)}$ in the form of series expansion:[103]

$$F_x^{(p)} = \frac{3p_d^2}{2\varepsilon_n L^4} + \frac{p_d^4}{2\pi\gamma\varepsilon_n^2 r_c^9}\,f_x^{(p)}\,, \qquad (15.109)$$

$$f_x^{(p)} = -\frac{27}{320}\left(\frac{r_c}{L}\right)^4 + \frac{1}{256}\left(\frac{r_c}{L}\right)^5 + \frac{213}{512}\left(\frac{r_c}{L}\right)^6 - \frac{271}{256}\left(\frac{r_c}{L}\right)^7$$
$$+\frac{2099}{4096}\left(\frac{r_c}{L}\right)^8 + \left[\frac{2623}{256} - \frac{9}{16}\ln\left(\frac{r_c}{L}\right)\right]\left(\frac{r_c}{L}\right)^9 + O\left(\frac{r_c^{10}}{L^{10}}\right). \qquad (15.110)$$

Combining Equations 15.104, 15.105 and 15.109, 15.110 we finally obtain an expression for the total interaction force, F_x, acting on the right-hand-side particle B, in the form of an asymptotic expansion:

$$F_x = \frac{3p_A^2}{2\varepsilon_n L^4}\left[1 - \frac{2\delta}{5} + \frac{5\delta}{2}\left(\frac{r_c}{L}\right)^2 - \frac{15\delta}{2}\left(\frac{r_c}{L}\right)^3 + \frac{175\delta}{32}\left(\frac{r_c}{L}\right)^4 + \ldots\right]\,, \qquad (15.111)$$

where $\delta = \tan\psi_c$ is the meniscus slope at the contact line given by Equation 15.94. The first term in the right-hand side of Equation 15.111 corresponds to the force of direct electric repulsion, F_{ED}, between two charged particles adsorbed at a planar liquid interface ($\delta = 0$), whereas the sum of all other terms in Equation 15.111 (those $\propto \delta$) gives the electrocapillary force, F_{EC}; see also Figure 15.3 and Equations 15.14 through 15.16. Note that for long distances ($L/r_c >> 1$), F_{EC} is negative (attractive) thanks to the contribution from the leading term in $f_x^{(p)}$; see Equation 15.110. However, $\delta < 1$, and then the total force, F_x, is positive

(repulsive). Thus, for the considered system, in the region where the asymptotic expansion, Equation 15.111 is applicable, the electrostatic repulsion between the two like-charged particles prevails over the capillary attraction. In the next section, we demonstrate that in another case the capillary attraction can prevail.

15.6 HYBRID ELECTRO-GRAVITY-INDUCED CAPILLARY ATTRACTION

15.6.1 Interaction between Two Floating Particles: Experiment

Experiments with hydrophobized glass spheres of radii (R) in the range of 200–300 μm, which are attached to the boundary tetradecane/water, were carried out in Ref. 61. Such particles are moving toward each other under the action of attractive force, whose physical origin was investigated. An illustrative example is given in Figure 15.10. Two different procedures of particle hydrophobization were used, which lead to obtaining uncharged and charged particles.[61] To establish whether a given particle was charged or uncharged, the meniscus-slope angle ψ_c was measured from side-view photographs of the particles, like those in Figure 15.4. For uncharged particles, the experimental angle ψ_c is small and equal to the calculated gravitational angle, ψ_g (see, e.g., Figure 15.4a). For charged particles, the experimental angle ψ_c is markedly larger than ψ_g (Figure 15.4b). The reason to work with particle radii 200–300 μm is that for such particles the angle ψ_c can be measured with a good accuracy, which is difficult for smaller particles.

To confirm that the electric field of the particles with $\psi_c >> \psi_g$ is really due to surface electric charges (rather than dipoles), in independent control experiments we inserted two electrodes in the form of parallel metal plates in the oily phase. The lower edge of each electrode was situated close to the oil/water interface without touching it. When a particle (with $\psi_c >> \psi_g$) is present at the liquid interface between the electrodes, it moves toward one of them, usually toward the cathode. If the polarity of the electrodes is exchanged, the particle moves toward the other electrode. This is the behavior of a particle with positive surface charge, rather than behavior of a dipole.[104]

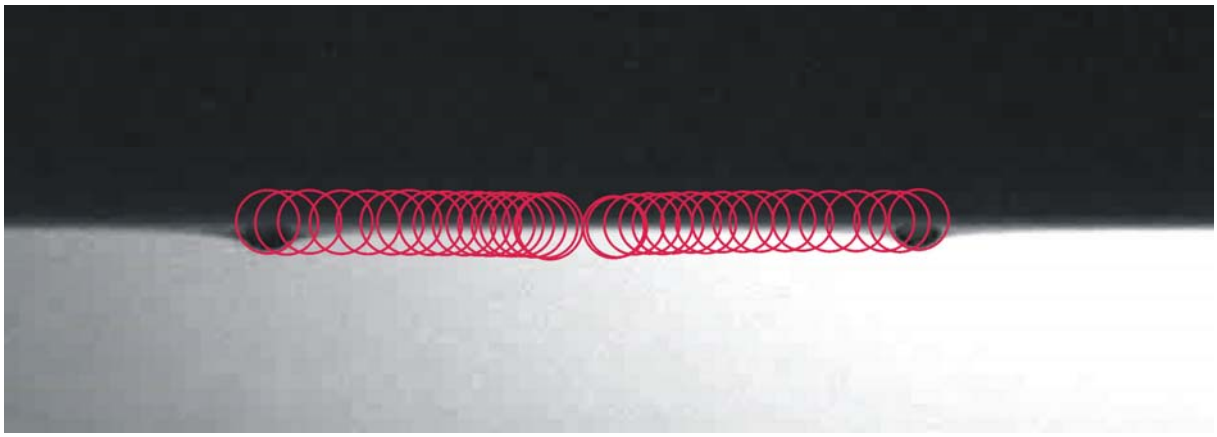

FIGURE 15.10 A side-view photograph of two hydrophobized glass particles of radius ≈ 300 μm at the interface between tetradecane and water solution of 50 mM sodium dodecyl sulfate (SDS) + 50 mM NaCl. The circles represent consecutive positions of the two particles, which are moving toward each other under the action of an attractive force.

In experiments like that illustrated in Figure 15.10, the center-to-center distance between the two particles was recorded as a function of time, that is, $L = L(t)$.[61] The purpose of these experiments was to check whether the particle motion is influenced by any electric field-induced capillary attraction. For this reason, control experiments with uncharged particles were carried out. Illustrative experimental results are shown in Figure 15.11 for four pairs of particles. For uncharged adsorbed particles, the attraction between them can be attributed to the action of the gravity-induced capillary force, which is theoretically described by Equation 15.5. For this reason, the experimental distance, $L(t)$, was fitted by means of the equation:[61]

$$\frac{\mathrm{d}L}{\mathrm{d}t} = -\frac{2}{\beta_{\mathrm{m}} f_{\mathrm{h}}} F_x, \quad \text{where} \quad F_x = \frac{F_z^{(\mathrm{g},1)} F_z^{(\mathrm{g},2)}}{2\pi\gamma} q K_1(qL) \tag{15.112}$$

Here, $F_z^{(\mathrm{g},1)}$ and $F_z^{(\mathrm{g},2)}$ are the vertical gravitational forces (weight minus Archimedes force) acting on the first and second particle; β_{m} is the mean hydrodynamic resistance; and f_{h} is a drag coefficient that is given by the Stimson–Jeffrey formula.[61,104] The expression for F_x in Equation 15.112 follows from Equation 15.5 and from the vertical force balance, $F_z^{(\mathrm{g},j)} = 2\pi\gamma r_{\mathrm{c}} \sin\psi_{\mathrm{c},j} = 2\pi\gamma Q_j$ (j = 1, 2), where Q_j is given by Equation 15.7. The solid lines in Figure 15.11 represent the best fits of the data by means of Equation 15.112. The excellent agreement between theory and experiment indicates that the attraction between the uncharged particles is really due to the gravity-induced lateral capillary force. A single adjustable

parameter, β_m, was used in these fits, and the obtained parameter values agree very well with the theoretical estimates; see Refs. 61 and 104 for details.

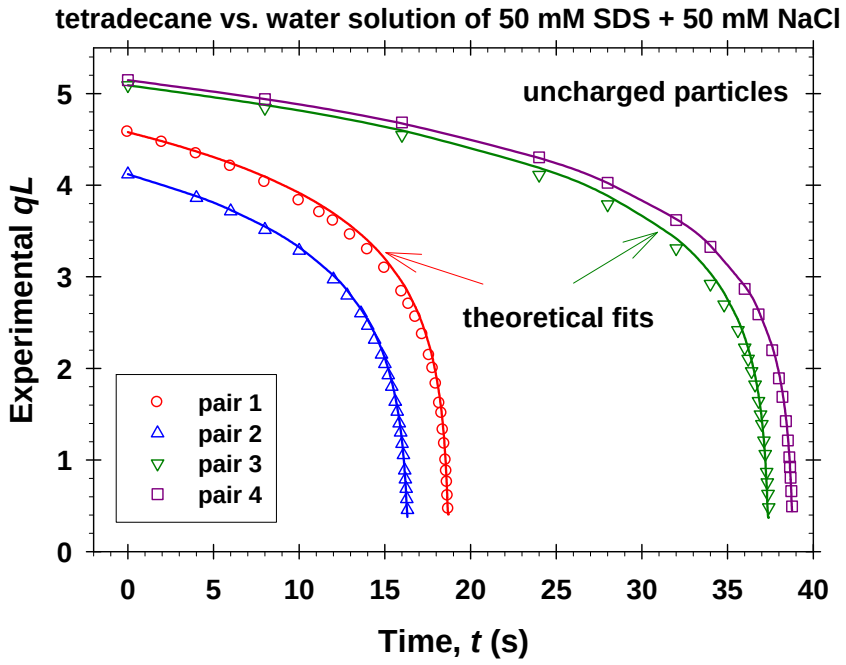

FIGURE 15.11 Experimental time-dependences of the interparticle center-to-center distance, $L(t)$, measured for four pairs of uncharged hydrophobic spherical particles attached to the interface between tetradecane and water solution of 50 mM SDS + 50 mM NaCl. The data points are from Ref. 61 and the theoretical fits are drawn by means of Equation 15.112.

Figure 15.12 shows a typical set of data from Ref. 61 for two electrically charged particles, for which $\psi_{c,j} >> \psi_{g,j}$ (j = 1, 2). To see whether the charge of the particles influences their motion, we calculated what would be the distance $L(t)$ if gravity alone were responsible for the particle motion – see the upper long-dash curve in Figure 15.12. The difference between the latter curve and the experimental points indicates that the charge of the particles leads to acceleration of their motion toward each other.

We also took into account also the fact that there is a meniscus on the walls of the experimental cell (the oil/water interface does not meet the vertical wall at 90°). This leads to the formation of a slightly concave oil/water interface (meniscus). The slope of this meniscus near the center of the cell (where the investigated particles are located) is rather small, but it still could accelerate the particle motion. The dash-dot line in Figure 15.12 is calculated by taking into account this effect. We see that the influence of the meniscus on the wall on the particle motion is relatively weak, and cannot explain the experimental data.[104]

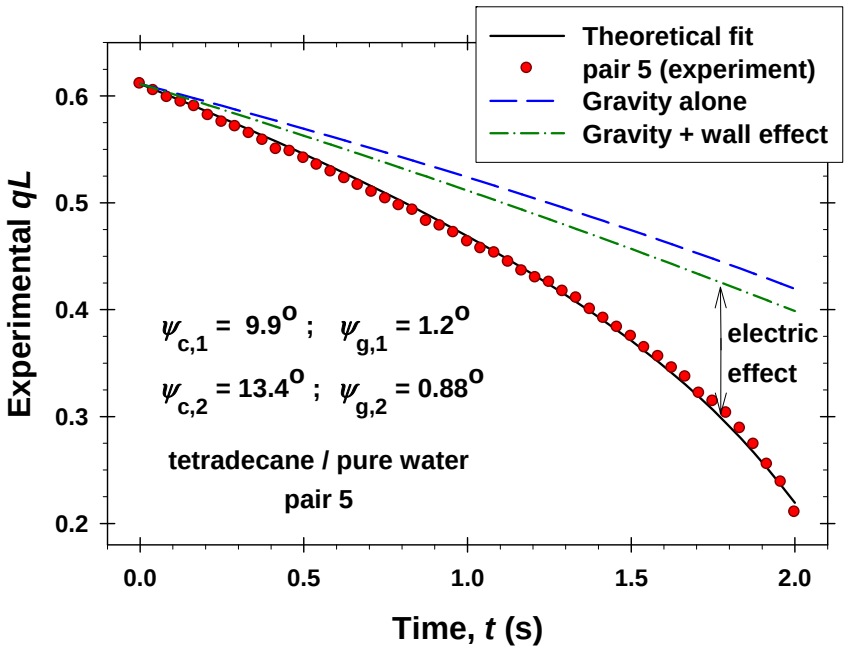

FIGURE 15.12 Experimental time-dependence of the interparticle center-to-center distance, $L(t)$, measured for a pair of charged hydrophobic spherical particles attached to the interface between tetradecane and water; $\psi_{c,1}$ and $\psi_{c,2}$ are the experimental values of the meniscus slope angle for the two particles, whereas $\psi_{g,1}$ and $\psi_{g,2}$ are the respective calculated values for uncharged particles (gravity force alone). The data points are from Ref. 61 and the theoretical fit is drawn by means of Equation 15.130. The calculated upper long-dash curve shows what would be the distance $L(t)$ if gravity alone were responsible for the particle motion. The dash-dot line is calculated by taking into account also the slight concavity of the interface due to the meniscus on the wall.

Note that the data in Figure 15.12 indicates the action of an additional attraction, which is stronger than the direct electric repulsion between the two like-charged particles. Moreover, this additional attraction is rather long-ranged as compared to the range of the electrostatic meniscus deformations observed in Ref. 60. We tried various ways to interpret these results. We found only one model, which can explain the experimental data. This model, developed in Ref. 104, is briefly described in the next section.

15.6.2 Overlap of Gravitational and Electric Interfacial Deformations

Theoretical expressions derived in Section 15.3 allow us to make (relatively easy) estimates of the range of the lateral capillary force between two adsorbed particles. In view of Equations 15.38 and 15.44, we could expect that

$$F_x^{(C)} \propto \gamma \int_{-\infty}^{\infty} \mathrm{d}y \frac{\partial \zeta_1}{\partial y} \frac{\partial \zeta_2}{\partial y}\bigg|_{x=0}, \tag{15.113}$$

where we have substituted $\zeta_A = \zeta_1$ and $\zeta_B = \zeta_2$. For purely gravitational meniscus, we have $\partial\zeta_i/\partial r \propto K_1(qr) \propto 1/r$, $i = 1,2$, and then Equation 15.113 yields $F_x^{(C)} \propto 1/L$, in agreement with Equation 15.6. Likewise, for two similar capillary quadrupoles we have $\partial\zeta_i/\partial r \propto 1/r^3$, $i = 1,2$, and then Equation 15.113 yields $F_x^{(C)} \propto 1/L^5$, in agreement with Equation 15.79 for $m = n = 2$. One could check that the same approach gives correctly the asymptotic behavior of the force of interaction between two capillary multipoles of arbitrary orders.

For a particle with isotropic distribution of the surface charge (Figure 15.13a), due to the image-charge effect, the particle's electric field has asymptotically dipolar character. It was established, both theoretically and experimentally,[60] that in such a case $\zeta_1 \propto 1/r^4$, and consequently, $\partial\zeta_1/\partial r \propto 1/r^5$. Let us assume that the latter interfacial deformation overlaps with the gravitational deformation around the second particle, that is, $\partial\zeta_2/\partial r \propto 1/r$. Then, Equation 15.113 yields $F_x^{(C)} \propto 1/L^5$. The latter capillary force decays faster than the direct electric repulsion between the two particles, $F_{\mathrm{ER}} \propto 1/L^4$; see Equation 15.12. Hence, it cannot explain the experimental results (Figure 15.12).

Next, let us consider a particle with anisotropic distribution of the surface charge (Figure 15.13b). Due to the image-charge effect, the electric field of such particle can be modeled as a pair of dipoles directed along the z-axis and separated at a distance $2s_y$. The anisotropy of the particle's electric field gives rise to anisotropic electric field-induced deformation of the liquid interface around the particle, which is equivalent to a capillary quadrupole; see Equation 15.122 below. For a capillary quadrupole, we have $\partial\zeta_1/\partial r \propto 1/r^3$. The latter interfacial deformation overlaps with the gravitational deformation around the second particle, for which $\partial\zeta_2/\partial r \propto 1/r$. Then, Equation 15.113 yields $F_x^{(C)} \propto 1/L^3$. The latter capillary force decays slower than the direct electric repulsion between the two particles, $F_{\mathrm{ER}} \propto 1/L^4$. Below, we demonstrate that it can quantitatively explain the experimental results (Figure 15.12).

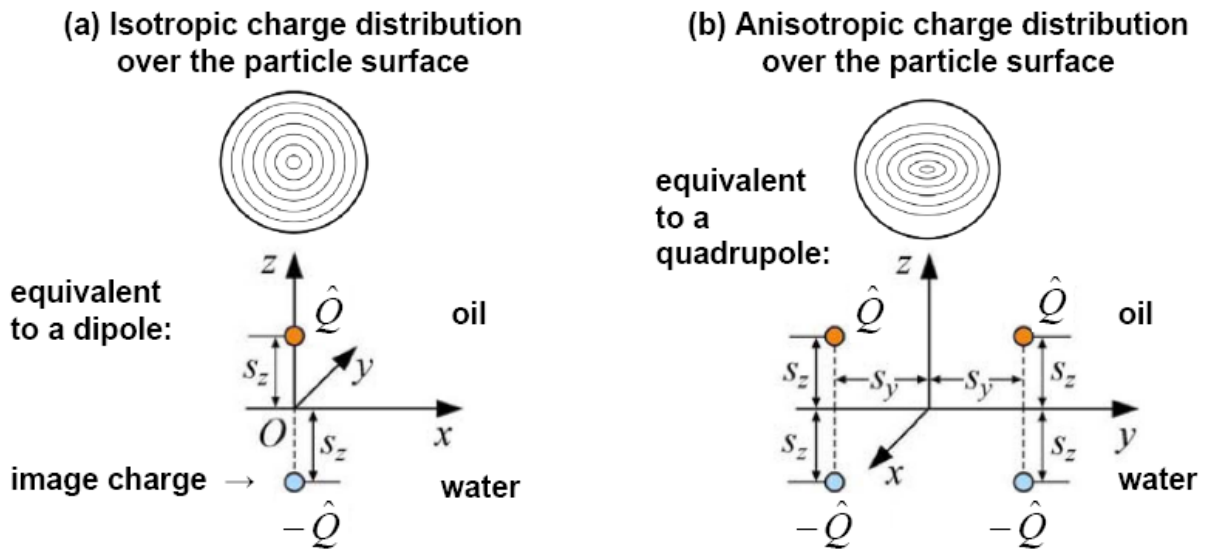

FIGURE 13 Modeling of charged particles attached to an oil/water interface. (a) If the distribution of the surface charges is isotropic, the particle can be modeled as a dipole (see also Figure 15.5). (b) If the surface-charge distribution is anisotropic, the particle can be modeled as a pair of two parallel dipoles.

Following Ref. 104, let us consider the interaction between two identical particles of anisotropic surface-charge distribution. The potential of the electric field created by the considered quadrupolar configuration (Figure 15.13b) in the nonpolar fluid is:

$$\varphi_0 = \frac{\hat{Q}}{\varepsilon_n}[x^2 + (y - s_y)^2 + (z - s_z)^2]^{-1/2} + \frac{\hat{Q}}{\varepsilon_n}[x^2 + (y + s_y)^2 + (z - s_z)^2]^{-1/2}$$

$$-\frac{\hat{Q}}{\varepsilon_n}[x^2 + (y - s_y)^2 + (z + s_z)^2]^{-1/2} - \frac{\hat{Q}}{\varepsilon_n}[x^2 + (y + s_y)^2 + (z + s_z)^2]^{-1/2}, \quad (15.114)$$

where $\hat{Q}$ denotes electric charge. In Equation 15.114, the planes of the two quadrupoles are parallel to the vertical *yz*-plane, which is perpendicular to the *x*-axis that connects the two particles (Figure 15.13b). This configuration is stable, because of the interparticle electrostatic repulsion.

In zero-order approximation, the Laplace Equation of capillarity (Equation 15.87) acquires the form:

$$\frac{1}{r}\frac{\partial}{\partial r}\left(r\frac{\partial \zeta}{\partial r}\right) + \frac{1}{r^2}\frac{\partial^2 \zeta}{\partial \phi^2} = -\frac{\varepsilon_n}{8\pi\gamma}\left(\frac{\partial \varphi_0}{\partial z}\right)^2\Bigg|_{z=0}, \quad (15.115)$$

where polar coordinates, (r,ϕ), have been introduced in the xy-plane. The boundary conditions are:

$$\zeta = 0 \quad \text{at} \quad r = r_c\,; \qquad\qquad \zeta \to h_c \quad \text{at} \quad r \to \infty\,. \tag{15.116}$$

The boundary condition at $r = r_c$ corresponds to fixed contact line at the particle surface. This is a realistic boundary condition, because contact angle hysteresis is usually present at solid surfaces, the absence of hysteresis being exclusion.[134–140] We will seek the solution of Equation 15.115 in the form:

$$\zeta(r,\phi) = \xi_0(r) + \xi_2(r)\cos(2\phi)\,. \tag{15.117}$$

From Equations 15.114, 15.115 and 15.117 we obtain the following equations for the coefficient functions:[104]

$$\frac{1}{r}\frac{\mathrm{d}}{\mathrm{d}r}\left(r\frac{\mathrm{d}\xi_0}{\mathrm{d}r}\right) = -\frac{\hat{Q}^2 s_z^2}{\pi\gamma\varepsilon_n}\frac{2(r^2+s_y^2+s_z^2)^2+15s_y^2r^2}{(r^2+s_y^2+s_z^2)^5}, \tag{15.118}$$

$$\frac{1}{r}\frac{\mathrm{d}}{\mathrm{d}r}\left(r\frac{\mathrm{d}\xi_2}{\mathrm{d}r}\right) - \frac{4}{r^2}\xi_2 = \frac{\hat{Q}^2 s_z^2}{\pi\gamma\varepsilon_n}\frac{15s_y^2r^2}{(r^2+s_y^2+s_z^2)^5}, \tag{15.119}$$

$$\xi_0(r_c) = \xi_2(r_c) = 0; \quad \lim_{r\to\infty}\xi_0(r) = h_c\,; \quad \lim_{r\to\infty}\xi_2(r) = 0\,. \tag{15.120}$$

The solution of Equation 15.118, along with the boundary conditions (Equation 15.120) is:[104]

$$\xi_0 \approx h_c - \frac{\hat{Q}^2 s_z^2}{8\pi\gamma\varepsilon_n r^4} + \ldots \quad \text{for} \quad r >> r_c\,. \tag{15.121}$$

Because ξ_0 describes the interfacial deformation produced by isotropic electric field, we have $\xi_0 \propto 1/r^4$, as expected (see above). Furthermore, the general solution of Equation 15.119 reads:

$$\xi_2 = A_1 r^2 + \frac{A_2}{r^2} + \frac{5\hat{Q}^2 s_y^2 s_z^2(3r^2+s_y^2+s_z^2)}{32\pi\gamma\varepsilon_n r^2(r^2+s_y^2+s_z^2)^3}, \tag{15.122}$$

where A_1 and A_2 are constants of integration. From the boundary condition at $r \to \infty$, we obtain $A_1 = 0$. From the boundary condition at $r = r_c$, we obtain:

$$A_2 = -\frac{5\hat{Q}^2 s_y^2 s_z^2(3r_c^2+s_y^2+s_z^2)}{32\pi\gamma\varepsilon_n(r_c^2+s_y^2+s_z^2)^3} \tag{15.123}$$

In fact, the term A_2/r^2 in Equation 15.122 is the source of the long-range deformation, $\xi_2 \propto 1/r^2$, created by the four charges configuration in Figure 15.13b. This deformation

appears because the anisotropic electric field tends to produce a *saddle-shaped* meniscus around the particle, but the *isotropic* boundary condition for fixed contact line, $\xi_2(r_c) = 0$, must be preserved. This leads to a nonzero value of the coefficient A_2; see equation 15.123. For this reason, the higher-order quadrupolar term ξ_2 (Figure 15.13b) produces a deformation of longer range ($\xi_2 \propto 1/r^2$) than the dipolar term (Figure 15.13a), which yields $\xi_0 \propto 1/r^4$; compare Equations 15.121 and 15.122, as well as Figures 15.13a and 15.13b. The asymptotic form of Equation 15.122 is:

$$\xi_2 = \frac{A_2}{r^2} + \frac{15\hat{Q}^2 s_z^2 s_y^2}{32\pi\gamma\varepsilon_n}\frac{1}{r^6} + \ldots \quad \text{for} \quad r >> r_c\,, \tag{15.124}$$

where A_2 is given by Equation 15.123.

The final result for the total interaction force between two different particles (particles 1 and 2) reads:[104]

$$F_x = \frac{F_z^{(g,1)} F_z^{(g,2)}}{2\pi\gamma} qK_1(qL) + 2F_z^{(g,1)}\frac{a_2^{(el)} r_{c2}^2}{L^3} + 2F_z^{(g,2)}\frac{a_1^{(el)} r_{c1}^2}{L^3}\,, \tag{15.125}$$

where terms $O(1/L^4)$ are neglected; r_{c1} and r_{c2} are the radii of the contact lines of the two particles; the quantities $a_1^{(el)}$ and $a_2^{(el)}$ are related to the electric field-induced interfacial deformations:

$$a_j^{(el)} \equiv h_j^{(el)} - h_j^{(wall)} \qquad (j = 1,2)\,, \tag{15.126}$$

$$h_j^{(el)} \equiv \frac{15F_z^{(el,j)}}{32\pi\gamma}\frac{s_{y,j}^2}{b_j^2}\,, \tag{15.127}$$

$$F_z^{(el,j)} = \frac{p_{dj}^2}{16\varepsilon_n b_j^4}\,, \qquad b_j^2 \equiv r_{c,j}^2 + s_{y,j}^2 + s_{z,j}^2\,. \tag{15.128}$$

Here, $p_{dj} = 4\hat{Q}_j s_{z,j}$ is the particle dipole moment (see Figure 15.13b); $s_{y,j}$ and $s_{z,j}$ (j = 1, 2) are the values of s_y and s_z for the two different particles; $F_z^{(el,j)}$ is the electrodipping force acting on the respective particle. For $s_{z,j} \to 0$, Equation 15.128 reduces to Equation 15.95. The effect of the meniscus on the wall of the experimental cell, induces a small repulsive quadrupolar term, which is also taken into account through $h_1^{(wall)}$ and $h_2^{(wall)}$:

$$h_j^{(wall)} = \frac{qr_{cj}^2 \tan\psi_w}{4\sinh(qb_c/2)} \qquad (j = 1,2)\,, \tag{15.129}$$

where ψ_w is the meniscus slope angle at the wall of the experimental cell, and b_c is the width of the cell (the shorter side of the rectangular horizontal section of the experimental cell).

In view of Equation 15.112, the first term in the right-hand side of Equation 15.125 is the gravity-induced lateral capillary force; the second and the third terms express a hybrid electro-gravity-induced capillary force, which is due to the interaction between a gravity-induced capillary charge and an electric field-induced capillary quadrupole. Finally, the distance $L(t)$ between the two particles can be determined by integrating the equation:[104]

$$\frac{\mathrm{d}L}{\mathrm{d}t} = -\frac{2}{\beta_m f_h}\left[F_x + \frac{(F_z^{(g,1)} + F_z^{(g,2)})\tan\psi_w}{4\sinh(qa_c/2)}qL\right], \qquad (15.130)$$

where the last correction term accounts for the sliding of the particle along the meniscus on the wall; a_c is the long side of the base of the experimental cell; F_x is given by Equation 15.125.

The solid lines in Figure 15.14 represent the best fits of experimental data from Ref. 61 by means of Equation 15.130. For simplicity, it was assumed that $s_{y,1}/b_1 = s_{y,2}/b_2 = s_y/b$. The two adjustable parameters, which have been varied to fit each experimental curve, are s_y/b and ψ_w. All other parameters are known from the experiment. In particular, the electrodipping force in Equation 15.127 was calculated from experimentally determined quantities: $F_z^{(el,j)} = 2\pi\gamma r_c \sin\psi_{c,j}$, $j = 1, 2$. The coefficients of hydrodynamic resistance, β_1 and β_2, were calculated as explained in Ref. 61. As a result, we obtained values of s_y/b in the range 0.20–0.35, which is reasonable; see Figure 15.13b. From the determined parameter values, we estimated the term $h_j^{(wall)}$ in Equation 15.126, which turned out to be really a small correction.

The anisotropy of the surface charge ($s_y/b > 0$) and some scattering of the obtained s_y/b values could be explained with the relatively low value of the surface charge density, σ_{pn}, at the particle/nonpolar-fluid interface. Indeed, the average value $\sigma_{pn} \approx 70$ μC/m^2 (determined for this type of particles in Refs. 58 and 60) is equivalent to an average distance of 480 Å between two surface charges assuming square packing. Under such conditions, we can expect that the energy of repulsion between the adsorbed ions is much smaller than their adsorption energies, which would lead to deviations from uniform and isotropic surface charge distribution. In Figure 15.14, the agreement between the experimental points and the

theoretical curves is excellent, which indicates that the experimentally observed strong attraction in this system can be really attributed to the interplay of gravitational and electric field-induced deformations in the liquid interface and to the resulting hybrid capillary force.

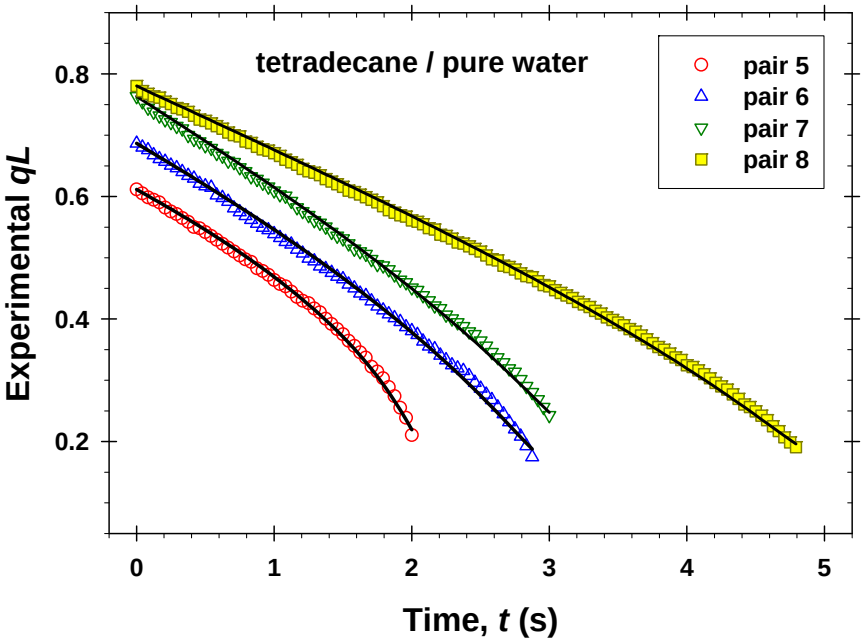

(a)

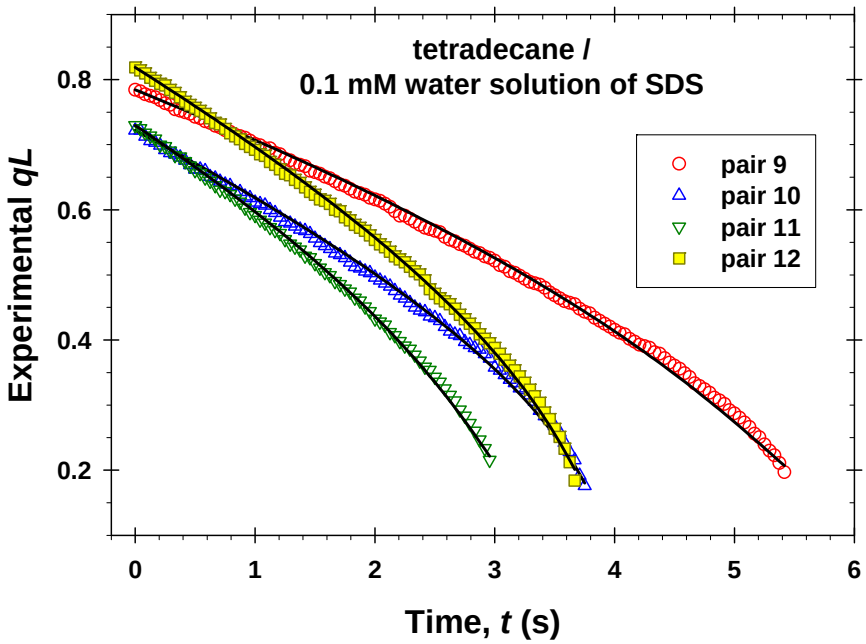

(b)

FIGURE 14 Plots of the dimensionless distance between two particles, qL versus time, (t). The experimental points are data from Ref. 61 with the same numbers of the pairs of particles. The solid lines represent the best fits of the data by means of Equation 15.130. (a) The aqueous phase is pure water; $q^{-1} = 4.74$ mm. (b) The aqueous phase is water solution of 0.1 mM sodium dodecyl sulfate (SDS); $q^{-1} = 4.35$ mm.

15.7 CONCLUDING REMARKS

The capillary forces between particles at a liquid interface, that is, the long-range interparticle interactions mediated by the interface, are universal in three aspects: (i) particle nature; (ii) particle size and (iii) particle shape.

With respect to the particle's chemical nature, the capillary forces are operative between both inorganic and organic particles, including biological objects such as cells and viruses.[9,25,26] The particle is only important to create deformation in the liquid interface when it is attached to it, or when it is captured in a liquid film (see Section 15.2).

With respect to the particle size, the lateral capillary forces are observed for particle diameters from several nanometers to several centimeters. This includes both the "nanoworld" (1 nm–1 μm) and the "mesoworld" (1 μm–1 mm). In the mesoworld, the gravity-induced capillary force is powerful, whereas the Brownian motion is negligible. In contrast, in the nanoworld, the Brownian motion becomes essential, but the gravity-induced capillary force is completely negligible. Then, the immersion-type capillary forces (Sections 15.2.4 through 15.2.6) and the electric field-induced interactions[90,91] could come into play. Here (Section 15.5) we considered only the case of charges located at the particle/nonpolar-fluid interface. The capillary forces due to charges at the particle/water interface, which are expected to be significant in the nanoworld,[58] need additional investigation. Hybrid, electro-gravity-induced capillary force was found to engender a powerful attraction in the mesoworld[61,104] (Section 15.6).

With respect to the particle shape, the capillary forces are operative between both perfect colloidal spheres and between particles of angular and irregular shape (Sections 15.2.2 and 15.4). In the latter case, the particle shape leads to the formation of undulated or irregular contact line, which induces deformations in the surrounding liquid interface. In such a case, we are dealing with the so-called capillary multipoles. Theoretical expressions for the interactions between capillary multipoles of arbitrary orders, derived by means of the general approach from Section 15.3, are given in Section 15.4. Moreover, as demonstrated in Section 15.6, particles, which represent electric multipoles, induce capillary multipoles because their electric field creates anisotropic deformations in the surrounding liquid interface.

The possible applications of the capillary forces in material science are numerous. This includes "bottom-up" approaches based on particle self-assembly under the action of capillary force such as the convective self-assembly method.[11,12,25,141,142] In addition, self-

assembled structures can be used in "top-down" approaches for lithographic masks,[32] microcontact printing,[31] antireflective coatings,[22] etc. The great scientific and practical importance of the lateral capillary forces will certainly stimulate future research in this field.

Acknowledgements

A partial support from EU COST Action D43 "Colloid and Interface Chemistry for Nanotechnology" and from Project DO-02-121 of NSF-Bulgaria is gratefully acknowledged. The authors are thankful to Ms. Mariana Paraskova for her assistance in the Figure preparation.

References

1. Nicolson, M. M. *Proc. Cambridge Philos. Soc*. 1949, *45*, 288–295.
2. Derjaguin, B. V., Starov, V. M. *Colloid J. USSR Engl. Transl.* 1977, *39*, 383–386.
3. Chan, D. Y. C., Henry, J. D., White, L. R. *J. Colloid Interface Sci*. 1981, *79*, 410–418.
4. Kralchevsky, P. A., Paunov, V. N., Ivanov, I. B., Nagayama, K. *J. Colloid Interface Sci.* 1992, *151*, 79–94.
5. Kralchevsky, P. A., Paunov, V. N., Denkov, N. D., Ivanov, I. B., Nagayama, K. *J. Colloid Interface Sci*. 1993, *155*, 420–437.
6. Paunov, V. N., Kralchevsky, P. A., Denkov, N. D., Nagayama, K. *J. Colloid Interface Sci*. 1993, *157*, 100–112.
7. Kralchevsky, P. A., Nagayama, K. *Langmuir* 1994, *10*, 23–36.
8. Kralchevsky, P. A., Nagayama, K. *Adv. Colloid Interface Sci.* 2000, *85*, 145–192.
9. Kralchevsky, P. A., Nagayama, K. *Particles at Fluid Interfaces and Membranes*, Elsevier, Amsterdam, 2001.
10. Kralchevsky, P. A., Denkov, N. D. *Curr. Opin. Colloid Interface Sci*. 2001, *6*, 383–401.
11. Denkov, N. D., Velev, O. D., Kralchevsky, P. A., Ivanov, I. B., Yoshimura, H., Nagayama, K. *Langmuir* 1992, *8*, 3183–3190.
12. Denkov, N. D., Velev, O. D., Kralchevsky, P. A., Ivanov, I. B., Yoshimura, H., Nagayama, K. *Nature* 1993, *361*, 26.
13. Matsushita, S. I., Yagi, Y., Miwa, T., Tryk, D. A., Koda T, Fujishima A. *Langmuir* 2000, *16*, 636–642.
14. Jiang, P., Sun, C.-H., Linn, N. C., Ho, B. J., Venkatesh, S. *Current Nanoscience* 2007, *3*, 296–305.
15. Rossi, R. C., Lewis, N. S. *J. Phys. Chem. B* 2001, *105*, 12303–12318.

16. Wang, D., Rogach, A. L., Caruso, F. *Chemistry of Materials* 2003, *15*, 2724–2729.

17. Matsushita, S., Miwa, T., Tryk, D. A., Fujishima, A. *Langmuir* 1998, *14*, 6441–6447.

18. Lytle, J. C., Yan, H., Ergang, N. S., Smyrl, W. H., Stein, A. *J. Materials Chem.* 2004, *14*, 1616–1622.

19. Park, S. H., Xia, Y. *Langmuir* 1999, *15*, 266–273.

20. Fu, H.-B., Yao, J.-N. *J. Am. Chem. Soc.* 2001, *123*, 1434–1439.

21. Fan, F., Stebe, K. J. *Langmuir* 2004, *20*, 3062–3067.

22. Ray, M. A., Li, J. *Adv. Mater.* 2007, *19*, 2020–2022.

23. Keddie, J. L. *Mater. Sci. Eng*. 1997, *21*, 101–170.

24. Beetsma, J. *Pigment Resin Technol.* 1998, *27*, 12–19.

25. Yamaki, M., Higo, J., Nagayama, K. *Langmuir* 1995, *11*, 2975–2978.

26. Nagayama, K. *Colloids Surf. A* 1996, *109*, 363–74.

27. Xiao, Y., Ju, H.-X., Chen, H.-Y. *Analytica Chimica Acta* 1999, *391*, 73–82.

28. Liu, Y., Li, Y. F., Huang, C. Z. *Rev. Analyt. Chem*. 2004, *23*, 75–85.

29. Holownia, P., Perez-Amodio, S., Price, C. P. *Analyt. Chem.* 2001, *73*, 3426–3431.

30. Kim Thanh, N. T., Rosenzweig, Z. *Analyt. Chem.* 2002, *74*, 1624–1628.

31. Xia, Y., Tien, J., Qin, D., Whitesides, G. M. *Langmuir* 1996, *12*, 4033–4038.

32. Burmeister, F., Schäfle, C., Keilhofer, B., Bechinger, C., Boneberg, J., Leiderer, P. *Adv. Mater.* 1998, *10*, 495–497.

33. Celio, H., Barton, E., Stevenson, K. J. *Langmuir* 2006, *22*, 11426–11435.

34. Xu, H., Goedel, W.A. *Angewandte Chemie - International Edition* 2003, *42*, 4694–4696.

35. Yuan, Z., Burckel, D. B., Atanassov, P., Fan, H. *J. Materials Chem.* 2006, *16*, 4637–4641.

36. Kuncicky, D. M., Bose, K., Costa, K. D., Velev, O. D. *Chem. Mater.* 2007, *19*, 141–143.

37. Vassileva, N. D., van den Ende, D., Mugele, F., Mellema, J. *Langmuir* 2005, *21*, 11190–11200.

38. Danov, K. D., Pouligny, B., Kralchevsky, P. A. *Langmuir* 2001, *17*, 6599–6609.

39. Dushkin, C.D., Nagayama, K., Miwa, T., Kralchevsky, P.A. *Langmuir* 1993, *9*, 3695–3701.

40. Abkarian, M., Nunes, J., Stone, H. A. *J. Am. Chem. Soc.* 2004, 126, 5978–5979.

41. Malaquin, L., Kraus, T., Schmid, H., Delamarche, E., Wolf, H. *Langmuir* 2007, 23, 11513–11521.

42. Pauliac-Vaujour, E., Moriarty, P. *J. Phys. Chem. C,* 2007, 111, 16255–16260.

43. Kralchevsky, P. A., Paunov, V. N., Denkov, N. D., Nagayama, K. *J. Chem. Soc. Faraday Trans*. 1995, *91*, 3415–3432.

44. Kralchevsky, P. A. *Adv. Biophys.* 1997, *34*, 25–39.

45. Müller, M. M., Deserno, M., Guven, J. *Phys. Rev. E* 2007, *76*, 011921.

46. Lucassen, J. *Colloids Surf.* 1992, *65*, 131–137.

47. Bowden, N., Choi, I. S., Grzybowski, B. A., Whitesides, G. M. *J. Am. Chem. Soc*. 1999, *121*, 5373–5391.

48. Wolfe, D. B., Snead, A., Mao, C., Bowden, N. B., Whitesides, G. M. *Langmuir* 2003, *19*, 2206–2014.

49. Brown, A. B. D., Smith, C. G., Rennie, A. R. *Phys. Rev. E* 2000, *62*, 951–960.

50. Loudet, J. C., Alsayed, A. M., Zhang, J., Yodh, A. G. *Phys. Rev. Lett*. 2005, *94*, 018301.

51. Loudet, J. C., Yodh, A. G., Pouligny, B. *Phys. Rev. Lett.* 2006, *97*, 018304.

52. Lewandowski, E. P., Bernate, J. A., Searson, P. C., Stebe, K. J. *Langmuir* 2008, *24*, 9302–9307.

53. Lehle, H., Noruzifar, E., Oettel, M. *European Phys. J. E* 2008, *26*, 151–160.

54. Stamou, D., Duschl, C., Johannsmann, D. *Phy.s Rev. E* 2000, *62*, 5263–5272.

55. Kralchevsky, P. A., Denkov, N. D., Danov, K. D. *Langmuir* 2001, *17*, 7694–7705.

56. Danov, K. D., Kralchevsky, P. A., Naydenov, B. N., Brenn, G. *J. Colloid Interface Sci.* 2005, *287*, 121–134.

57. Nikolaides, M. G., Bausch, A. R., Hsu, M. F., Dinsmore, A. D., Brenner, M. P., Gay, C., Weitz, D. A. *Nature* 2002, *420*, 299–301.

58. Danov, K. D., Kralchevsky, P. A., Boneva, M. P. *Langmuir* 2004, *20*, 6139–6151.

59. Danov, K. D., Kralchevsky, P. A. *J. Colloid Interface Sci*. 2006, *298*, 213–231.

60. Danov, K. D., Kralchevsky, P. A., Boneva, M. P. *Langmuir* 2006, *22*, 2653–2667.

61. Boneva, M. P., Christov, N. C., Danov, K. D., Kralchevsky, P. A. *Phys. Chem. Chem. Phys.* 2007, *9*, 6371–6384.

62. Aveyard, R., Clint, J. H., Nees, D., Paunov, V. N. *Langmuir* 2000, *16*, 1969–1979.

63. Aveyard, R., Binks, B. P., Clint, J. H., Fletcher, P. D. I., Horozov, T. S., Neumann, B., Paunov, V. N., Annesley, J., Botchway, S. W., Nees, D., Parker, A. W., Ward, A. D., Burgesset, A. N. *Phys. Rev. Lett.* 2002, *88*, 246102.

64. Horozov, T. S., Aveyard, R., Clint, J. H., Binks, B. P. *Langmuir* 2003, *19*, 2822–2829.

65. Stancik, E. J., Kouhkan, M., Fuller, G. G. *Langmuir* 2004, *20*, 90–94.

66. Horozov, T. S., Aveyard, R., Binks, B. P., Clint, J. H. *Langmuir* 2005, *21*, 7407–7412.

67. Horozov, T. S., Binks, B. P. *Colloids Surf. A* 2005, *267*, 64–73.

68. *Colloidal Particles at Liquid Interfaces*, Binks, B. P., Horozov, T. S. (Eds.), Cambridge University Press, Cambridge, UK, 2006.

69. Leunissen, M. E., van Blaaderen, A., Hollingsworth, A. D., Sullivan, M. T., Chaikin, P. M. *Proc. Natl. Acad. Sci.* 2007, *104*, 2585–2590.

70. Leunissen, M. E., Zwanikken, J., van Roij, R., Chaikin, P. M., van Blaaderen, A. *Phys. Chem. Chem. Phys.* 2007, *9*, 6405–6414.

71. Kralchevsky, P. A., Ivanov, I. B., Ananthapadmanabhan, K. P., Lips, A. *Langmuir* 2005, *21*, 50–63.

72. Megens, M., Aizenberg, J. *Nature* 2003, *424*, 1014.

73. Foret, L., Würger, A. *Phys. Rev. Lett*. 2004, *92*, 058302.

74. Oettel, M., Domínguez, A., Dietrich, S. *Phys. Rev. E* 2005, *71*, 051401.

75. Oettel, M., Domínguez, A., Dietrich, S. *Langmuir* 2006, *22*, 846–847.

76. Danov, K. D., Kralchevsky, P. A. *Langmuir* 2006, *22*, 848–849.

77. Würger, A., Foret, L. *J. Phys. Chem. B* 2005, *109*, 16435–16438.

78. Oettel, M., Domínguez, A., Dietrich, S. *J. Phys: Condensed Matter* 2005, *17*, L337–L342.

79. Würger, A. *Europhys. Lett.* 2006, 75, 978–984**.**

80. Domínguez, A., Oettel, M., Dietrich, S. *Europhys. Lett.* 2007, 77, 68002.

81. Gómez-Guzmán, O., Ruiz-Garcia, J. *J. Colloid Interface Sci*. 2005, *291*, 1–6.

82. Chen, W., Tan, S., Ng, T.-K., Ford, W.T., Tong, P. *Phys. Rev. Lett*. 2005, 95, 218301.

83. Chen, W., Tan, S., Huang, Z., Ng, T.-K., Ford, W. T., Tong, P. *Phys. Rev. E* 2006, *74*, 021406.

84. Ngai, T., Auweter, H., Behrens, S.H. *Macromolecules* 2006, 39, 8171–8177.

85. Hartland, S., Hartley, R. W. *Axisymmetric Fluid-Liquid Interfaces,* Elsevier, Amsterdam, 1976.

86. Kralchevsky, P. A., Ivanov, I. B., Nikolov, A. D. *J. Colloid Interface Sci*. 1986, *112*, 108–120.

87. Janke, E., Emde, F., Lösch, F. *Tables of Higher Functions*, McGraw-Hill, New York, 1960.

88. Abramowitz, M., Stegun, I. A. *Handbook of Mathematical Functions,* Dover, New York, 1965.

89. Korn, G. A., Korn, T. M. *Mathematical Handbook*, McGraw-Hill, New York, 1968.

90. Aubry, N., Singh, P. *Phys. Rev. E* 2008, *77*, 056302.

91. Aubry, N., Singh, P., Janjua, M., Nudurupati, S. *Proc. Natl. Acad. Sci*. 2008, *105*, 3711–3714.

92. Bowden, N., Terfort, A., Carbeck, J., Whitesides, G. M. *Science* 1997, *276*, 233–235.

93. Danov, K. D., Kralchevsky, P. A. *Adv. Colloid Interface Sci*. 2010, *154*, 91–103.

94. Helseth, L. E., Muruganathan, R. M., Zhang, Y., Fischer, T. M. *Langmuir* 2005, *21*, 7271–7275.

95. Binks, B. P. *Curr. Opinion Colloid Interface Sci.* 2002, *7*, 21–41.

96. Landau L. D., Lifshitz, E. M. *Electrodynamics of Continuous Media*: Volume 8 (Course of theoretical physics), Pergamon Press, Oxford, 1960.

97. Jackson, J. D. *Classical Electrodynamics*, John Wiley & Sons, New York, 1962.

98. Danov, K. D., Kralchevsky, P. A., Ananthapadmanabhan, K. P., Lips, A., *Langmuir* 2006, *22* 106–115.

99. Philipse, A. P., Vrij, A. *J. Colloid Interface Sci.* 1989, *128*, 121–136.

100. Labib, M. E., Williams, R. *J. Colloid Interface Sci.* 1987, *115*, 330–338.

101. Petkov, J. T., Denkov, N. D., Danov, K. D., Velev, O. D., R. Aust, R., Durst, F. *J. Colloid Interface Sci*. 1995, *172*, 147–154.

102. Dhar, P., Prasad, V., Weeks, E. R., Bohlein, T., Fischer, T. M. *J. Phys. Chem. B* 2008, *112*, 9565–9567.

103. Danov, K. D., Kralchevsky, P. A. *J. Colloid Interface Sci*. 2010, *345*, 505–514.

104. Danov, K. D., Boneva, M. P., Christov, N. C, Kralchevsky, P. A., *Langmuir* 2009, *25*, 9129–9139

105. Camoin, C., Roussell, J. F., Faure, R., Blanc, R. *Europhys. Lett*. 1987, *3*, 449–457.

106. Velev, O. D., Denkov, N. D., Paunov, V. N., Kralchevsky, P. A., Nagayama, K. *Langmuir* 1993, *9*, 3702–3709.

107. Dushkin, C. D., Kralchevsky, P. A., Yoshimura, H., Nagayama, K. *Phys. Rev. Lett*. 1995, *75*, 3454–3457.

108. Dushkin, C. D., Kralchevsky, P. A., Paunov, V. N., Yoshimura, H., Nagayama, K. *Langmuir* 1996, 12, 641–651.

109. Dushkin, C. D., Yoshimura, H., Nagayama, K. *J. Colloid Interface Sci*. 1996, *181*, 657–660.

110. Di Leonardo, R., Saglimbeni, F., Ruocco, G. *Phys. Rev. Lett*. 2008, *100*, 106103.

111. Denkov, N. D., Yoshimura, H., Nagayama, K., Kouyama, T. *Phys. Rev. Lett.* 1996, *76*, 2354–2357.

112. Denkov, N. D., Yoshimura, H., Nagayama, K. *Ultramicroscopy* 1996, *65*, 147–158.

113. Denkov, N. D., Yoshimura, H., Kouyama, T., Walz, J., Nagayama, K. *Biophys. J.* 1998, *74*, 1409–1420.

114. Horozov, T. S., Aveyard, R., Clint, J. H., Neumann, B. *Langmuir* 2005, *21*, 2330–2341.

115. Kralchevsky, P. A., Paunov, V. N., Nagayama, K. *J. Fluid. Mech*. 1995, 299, 105–132.

116. Danov, K. D., Pouligny, B., Angelova, M. I., Kralchevsky, P. A. *Studies in Surface Science and Catalysis*, Vol. 132, Elsevier, Amsterdam, 2001; pp. 519–524.

117. Danov, K. D., Pouligny, B., Kralchevsky, P. A. *Langmuir* 2001, *17*, 6599–6609.

118. Velikov, K. P., Durst, F., Velev, O. D. *Langmuir* 1998, *14*, 1148–1155.

119. Aranda-Espinoza, H., Berman, A., Dan, N., Pincus, P., Safran, S. *Biophys. J.* 1996, *71*, 648–656.

120. Gil, T., Ipsen,, J. H., Mouritsen, O. G., Sabra M. C., Sperotto, M. M., Zuckermann, M. J. *Biochim. Biophys. Acta* 1998, *1376*, 245–266.

121. Mansfield, S. L., Gotch, A. J., Harms, G. S., Johnson, C. K., Larive, C. K. *J. Phys. Chem. B* 1999, *103*, 2262–2269.

122. Lagüe, P., Zuckermann, M. J., Roux, B., *Faraday Discuss.* 1999, *111*, 165–172.

123. Biscari, P., Bisi, F., Rosso, R., *J. Math. Biol.*, 2002, *45*, 37–56.

124. Bohinc, K., Kralj-Iglic, V., May, S., *J. Chem. Phys.* 2003, *119*, 7435–7444.

125. Müller, M. M., Deserno, M., Guven, J., *Europhys. Lett.* 2005, *69*, 482–488.

126. Brannigan, G., Brown, F. L. H. *Biophys. J.* 2006, *90*, 1501–1520.

127. Botelho, A. V., Huber, T., Sakmar, T. P., Brown, M. F. *Biophys. J.* 2006, *91*, 4464–4477.

128. Schmidt, U., Guigas, G., Weiss, M. *Phys. Rev. Lett*. 2008, *101*, 128104.

129. Rheinstädter M. C. *Biointerphases* 2008, *3*, FB83–FB90.

130. Ono, S., Kondo, S. Molecular theory of surface tension in liquids, In: *Handbuch der Physik,* vol. 10, S. Flügge (Ed.), Springer, Berlin, 1960; p. 134.

131. Brand, L. *Vector and Tensor Analysis*, Wiley, New York, 1947.

132. Verwey, E. J. W., Overbeek, J. Th. G. *The Theory of Stability of Lyophobic Colloids*, Elsevier, Amsterdam, 1948.

133. Tamm, I. E. *Fundamentals of the Theory of Electricity*, Mir Publishers, Moscow, 1979.

134. Bartell, F. E., Shepard, J. W. *J. Phys. Chem.* 1953, *57*, 211–215.

135. Johnson Jr., R. E., R.H. Dettre, R. H. In: *Surface and Colloid Science*, Vol. 2, E. Matijevic (Ed.), Wiley, New York, 1969; pp. 85–153.

136. Starov, V. M. *Adv. Colloid Interface Sci*. 1982, *39*, 147–173.

137. Marmur, A. *Adv. Colloid Interface Sci*. 1994, *50*, 121–141.

138. Marmur, A. *J. Colloid Interface Sci*. 1994, *168*, 40–46.

139. Drelich, J., Miller, J. D., Good, R. J. *J. Colloid Interface Sci*. 1996, *179*, 37–50.

140. Iliev, S. D. *J. Colloid Interface Sci*. 1997, 194, 287–300.

141. Dimitrov, A. S., Nagayama, K. *Langmuir* 1996, *12*, 1303–1311.

142. Prevo, B. G., Velev, O. D. *Langmuir* 2004, *20*, 2099–2107.